AIMS Mathematics, 10(7): 15302–15332.
DOI: 10.3934/math.2025686
Received: 28 May 2025
Revised: 16 June 2025
Accepted: 24 June 2025
Published: 02 July 2025

http://www.aimspress.com/journal/Math

Research article

Reliability analysis of independent Burr-X competing risks model based on improved adaptive progressively Type-II censored samples with applications

Refah Alotaibi[1], **Mazen Nassar**[2,3,*] **and Ahmed Elshahhat**[4]

[1] Department of Mathematical Sciences, College of Science, Princess Nourah bint Abdulrahman University, P.O. Box 84428, Riyadh 11671, Saudi Arabia

[2] Department of Statistics, Faculty of Science, King Abdulaziz University, Jeddah 21589, Saudi Arabia

[3] Department of Statistics, Faculty of Commerce, Zagazig University, Egypt

[4] Faculty of Technology and Development, Zagazig University, Zagazig 44519, Egypt

* **Correspondence:** Email: mmohamad3@kau.edu.sa, mezo10011@gmail.com.

Abstract: In the analysis of failure time data, researchers often encounter situations in which events arise from multiple mutually exclusive causes. This framework is commonly referred to as competing risks. Traditional methods are inadequate in such settings, as they typically assume the presence of a single type of failure and do not account for the influence of other competing events. This study investigates the competing risks model under an improved adaptive progressive Type-II censoring scheme, which is particularly beneficial in contexts where the duration of testing is critical. The lifetimes associated with competing risks are assumed to follow independent Burr-X distributions, a flexible model capable of accommodating a variety of data types. Both classical and Bayesian estimation methods are utilized to estimate the model parameters and the reliability function, a key metric in reliability assessment. Maximum likelihood estimates are computed numerically, and approximate confidence intervals are derived. For Bayesian inference, squared error and linear-exponential loss functions are employed. Given the complexity of the posterior distribution, Markov chain Monte Carlo techniques are utilized to obtain Bayesian estimates and construct Bayesian credible intervals. A comprehensive numerical analysis, which includes a simulation study and the examination of real competing risk datasets, is conducted to evaluate and compare the performance of the proposed estimation methods.

Keywords: Burr-X competing risk model; reliability function; improved adaptive progressive Type-II censoring; Bayesian estimation; MCMC technique
Mathematics Subject Classification: 62F10, 62F15, 62N01, 62N05

1. Introduction

In numerous real-world scenarios, particularly within the fields of survival analysis and reliability engineering, it is often observed that the failure or death of individuals or items can be attributed to multiple potential causes. This phenomenon is widely recognized in statistical literature as the competing risks problem, where several risk factors compete to be the primary cause of the observed outcome. Consider the well-known example from Hoel [1], which stems from a laboratory experiment involving mice exposed to a dose of radiation at six weeks of age. In this study, the causes of death were categorized into three distinct groups: Thymic lymphoma, reticulum cell sarcoma, or other causes. This example serves as a classic illustration of the competing risks problem, where multiple potential causes of failure (in this case, death) are observed and analyzed. For additional examples of competing risks, refer to Crowder [2] and King [3]. In conventional analysis of competing risk datasets, the primary focus of the researcher is often on understanding the distribution of lifetimes associated with a specific cause of failure, such as Thymic lymphoma. In this approach, all other causes of failure are aggregated into a single category and treated as censored data, effectively disregarding their individual contributions to the overall failure process.

In recent years, significant improvements have been made in developing models aimed at evaluating the lifetimes associated with specific risks while accounting for the existence of competing risk factors. These competing risk models employ data encompassing both the failure time and an indicator variable delineating the particular cause of failure for an individual or item. The causes of failure in these models may be conceptualized as either independent or dependent. However, in the majority of instances, the analysis of competing risk data is predicated on the assumption that the causes of failure are independent see Kundu et al. [4]. The analysis of competing risk data has been extensively explored in numerous studies. For instance, notable contributions can be found in the works of Pintilie et al. [5], Zhang [6], El-Azeem et al. [7], and Tian et al. [8].

When analyzing competing risk data, researchers frequently encounter incomplete information regarding the lifetimes of all individuals or items under investigation. For instance, in clinical trials, participants may withdraw from the study, or the trial may conclude at a predetermined time point before all events are observed. Similarly, in industrial experiments, units may fail unexpectedly due to unforeseen circumstances. However, in many instances, the removal of units prior to failure is intentionally designed to optimize the testing process, thereby reducing both the time and costs associated with the experiment. The data acquired under such conditions are termed censored data. In the literature, one can find numerous censoring plans, each characterized by distinct features. One of the most commonly used censoring schemes in reliability and survival analysis is the progressive Type-II censoring (PT2C) plan. This approach allows for the removal of surviving units at various stages during the experiment. These removed units can subsequently be used for additional analysis or further investigations. For a deeper understanding of its applications and methodologies, readers may refer to the works of Balakrishnan and Sandhu [9], Balakrishnan et al. [10], Rastogi and Tripathi [11], Dey et al. [12], Krishna and Goel [13], Jeon et al. [14], and Kumari et al. [15].

Ng et al. [16] introduced a more adaptable censoring method called the adaptive progressive Type-II censoring (APT2C) scheme. This method not only generalizes the conventional PT2C plan but also improves the effectiveness of statistical inference when compared with other censoring plans. Nevertheless, Ng et al. [16] highlighted that the APT2C scheme is only efficient for statistical

inference when testing duration is not a limiting factor. For highly reliable units, this method can result in impractically long testing periods, rendering it inappropriate for scenarios where maintaining reasonable test lengths is essential. This censoring plan has been extensively employed in many studies, including those by Panahi and Asadi [17], Haj Ahmad et al. [18], and Elshahhat and Nassar [19], among others. To tackle this issue, Yan et al. [20] proposed the improved APT2C (IAPT2C) plan, which is particularly advantageous when managing the test duration is crucial. This refined approach generalizes various censoring methods, such as PT2C and APT2C, while ensuring that the experiments conclude within a predefined timescale, mitigating the issue of extended testing periods. For further insights into recent research on the IAPT2C strategy, refer to the studies by Elbatal et al. [21], Dutta and Kayal [22], and Irfan et al. [23]. Recently, Elshahhat and Nassar [24] studied the IAPT2C competing risks model in the case of Weibull distribution. The next section explores the IAPT2C scheme within the framework of a competing risks model.

One of the key challenges in modeling competing risk data is choosing an appropriate lifetime distribution that can accurately represent the failure times associated with different causes. Among the many flexible distributions available for such modeling, the Burr-X (BX) distribution stands out as a particularly versatile option. For the purpose of this analysis, we assume that the failure times follow the BX distribution. The BX distribution is part of the broader Burr family of distributions, originally introduced by Burr [25]. It is widely utilized in statistics and operations research, with applications spanning diverse fields such as medicine, agriculture, and biology. Despite having only one shape parameter, the BX distribution is capable of modeling a wide variety of data patterns. Its failure rate function is particularly noteworthy, as it can accommodate both increasing and bathtub-shaped failure rates, making it a powerful tool for analyzing complex datasets. For more applications regarding the BX distribution, see Tarvirdizade and Gharehchobogh [26], Rabie and Li [27], Kayid et al. [28], and Lio et al. [29], among others.

Considering the significance of the IAPT2C scheme in scenarios where the test duration and cost are critical, the relevance of the competing risks model for analyzing data involving multiple failure causes, and the versatility of the BX distribution in modeling diverse data types, we were motivated to undertake this study. These components have been widely studied individually; however, their integration within a unified inferential framework remains important. The primary objective of this study was to examine the competing risks model using data obtained under the IAPT2C scheme, assuming that the lifetimes associated with each competing risk are independently BX-distributed. This combination offers a novel approach to modeling complex reliability data under constrained experimental conditions. Our work contributes to the literature in the following ways.

(1) We extend the application of the BX distribution to the competing risks framework under IAPT2C censoring, an area that has primarily focused on simpler models such as exponential or Weibull distributions, see Dutta and Kayal [30], and Elshahhat and Nassar [24].
(2) We develop both frequentist (maximum likelihood estimates (MLEs) with approximate confidence intervals (ACIs)) and Bayesian inference methods (under the squared error (SE) and linear exponential (LINEX) loss functions) tailored to the IAPT2C competing risks BX setup.
(3) The estimation approach in this study goes beyond estimating only the model parameters, as is common in many existing works such as Wang and Li [31], Du and Gui [32], and Hassan et al. [33], among others. It is also extended to estimate the RF, which is one of the key reliability measures of interest.

(4) Due to the complexity of the posterior distribution, we implement a Markov Chain Monte Carlo (MCMC) algorithm to obtain Bayes estimates and Bayesian credible intervals (BCIs) for both parameters and the reliability function (RF) as a key reliability metric.
(5) We provide a comprehensive numerical evaluation through simulation studies and real data analysis, comparing classical and Bayesian approaches in terms of accuracy and stability under various censoring schemes.

By integrating these elements, our study addresses a gap in the current literature and provides a useful inferential framework for reliability practitioners dealing with complex failure mechanisms under constrained testing environments.

The organization of this paper is as follows: Section 2 provides an overview of the model's assumptions and descriptions. Section 3 focuses on deriving point and interval estimates for the parameters and the RF using the maximum likelihood method. In Section 4, Bayesian point and interval estimates are examined, with computations carried out using the MCMC technique. Section 5 presents a Monte Carlo simulation study to validate the proposed methods. Section 6 applies the methodologies to analyze real-world competing risk datasets. The paper concludes with a summary of the findings in Section 7.

2. Model description

For simplicity, we assume there are only two independent causes of failure, though the methods discussed in this paper can be readily extended to scenarios with more than two causes. Consider a life test involving n identical items, whose lifetimes are represented by independent and identically distributed (i.i.d.) random variables, $X_1, \ldots, X_n$. Under this setup, the failure of each unit is assumed to be influenced by one of the two competing risks. Thus, we have

$$X_i = min\left(X_{1i}, X_{2i}\right),\ i = 1, \ldots, n,$$

where X_{ri}, for $r = 1, 2$, denotes the latent failure time of the i-th unit under the r-th cause of failure. It is also assumed that the latent failure times X_{1i} and X_{2i}, for $i = 1, \ldots, n$ are independent. When a failure occurs, the failure time is recorded, and the specific cause of failure is identified by the indicator variable ϕ_i, where $\phi_i \in \{1, 2\}$. Here, $\phi_i = 1$ indicates that the i-th failure is due to the first cause, and $\phi_i = 2$ signifies that it is due to the second cause. This indicator variable $\phi_i, i = 1, \ldots, n$, helps determine the specific risk factor responsible for each observed failure. Assuming that $X_{ri}, r = 1, 2, i = 1, \ldots, n$, follows the BX distribution with the shape parameter θ_r, denoted as $BX(\theta_r), r = 1, 2$. Then, the probability density function (PDF), and cumulative distribution function (CDF) can be expressed, respectively, as

$$f_r(x; \theta_r) = 2\theta_j x e^{-x^2}\left(1 - e^{-x^2}\right)^{\theta_r - 1}, x > 0, \theta_r > 0, r = 1, 2, \tag{2.1}$$

and

$$F_r(x; \theta_r) = \left(1 - e^{-x^2}\right)^{\theta_r}. \tag{2.2}$$

At a given time t, the RF of $X_i = min(X_{i1}, X_{i2})$ can be obtained using (2.2) as follows:

$$R(t; \boldsymbol{\theta}) = \prod_{r=1}^{2}\left[1 - \left(1 - e^{-t^2}\right)^{\theta_r}\right], \tag{2.3}$$

where $\boldsymbol{\theta} = (\theta_1, \theta_2)^\top$.

The generation of an IAPT2C sample under competing risks can be outlined as follows: Let $m(< n)$ denote the required number of failures, and let $\mathbf{Q} = (Q_1, \ldots, Q_m)$ represent the predefined removal plan established before the experiment begins. The researcher also defines two threshold times, T_1 and T_2, where $T_1, T_2 \in (0, \infty)$ and $T_1 < T_2$. These points specify the experimental time boundaries: The test may move beyond T_1 but must conclude by T_2. This framework ensures that the experiment stays within a controlled duration while maintaining the adaptive nature of the censoring plan. At the failure of the i-th unit, with failure time $X_{i:m:n}$ for $i = 1, \ldots, m$, the researcher randomly withdraws Q_i units from the remaining surviving items. The cause of failure ϕ_i is recorded for each failure event. The process continues until the test ends under one of the following three scenarios:

- **Case I:** If the m-th failure occurs before the first threshold time T_1, i.e., $X_{m:m:n} < T_1$, the experiment is terminated at $X_{m:m:n}$. At this point, all remaining surviving items are removed from the test. This scenario results in the PT2C sample.
- **Case II:** If the first threshold time T_1 falls between the k_1-th and $(k_1 + 1)$-th failure times (i.e., $X_{k_1:m:n} < T_1 < X_{k_1+1:m:n}$, where k_1 represents the number of failures observed before T_1 and $(k_1 + 1) < m$) the removal pattern is adjusted. Specifically, no further items are removed after T_1 until the m-th failure occurs. This is achieved by setting $Q_{k_1+1} = \cdots = Q_{m-1} = 0$. The experiment concludes at the time of the m-th failure, and all remaining units are removed at that time. This scenario corresponds to the APT2C sample.
- **Case III:** If the m-th failure does not occur before the second threshold time T_2, i.e., $X_{m:m:n} > T_2$, the experiment is terminated at T_2. In this case, no items are removed after the first threshold T_1 is exceeded. Here, $k_2 < m$ represents the number of failures observed before T_2. At T_2, all remaining surviving units are removed, and the total number of removed units is given by $Q^\star = n - k_2 - Q_1 - \cdots - Q_{k_1}$.

Let $\underline{\mathbf{x}}$ represent an IAPT2C competing risks sample drawn from a continuous population. The sample can be expressed as

$$\underline{\mathbf{x}} = \{(x_1, \phi_1, Q_1), \ldots, (x_{k_1}, \phi_{k_1}, Q_{k_1}), (x_{k_1+1}, \phi_{k_1+1}, 0), \ldots, (x_{k_2}, \phi_{k_2}, 0), (T_2, Q^*)\},$$

where $x_i = x_{i:m:n}$ for simplicity. Based on this setup, the likelihood function of the observed data, excluding constant terms, can be formulated as

$$\begin{aligned} L(\boldsymbol{\theta}|\underline{\mathbf{x}}) \quad & \prod_{i=1}^{J} \left\{ \left[f_1(x_i;\theta_1)\bar{F}_2(x_i;\theta_2) \right]^{I(\phi_i=1)} \left[f_2(x_i;\theta_2)\bar{F}_1(x_i;\theta_1) \right]^{I(\phi_i=2)} \right\} \\ \times \quad & \prod_{i=1}^{M} \left\{ \left[\bar{F}_1(x_i;\theta_1)\bar{F}_2(x_i;\theta_2) \right]^{Q_i} \right\} \left[\bar{F}_1(\tau;\theta_1)\bar{F}_2(\tau;\theta_2) \right]^{Q^\star}, \end{aligned} \tag{2.4}$$

where $\bar{F}_r(.) = 1 - F_r(.)$,

$$I(\phi_i = r) = \begin{cases} 1 & \text{if } \phi_i = r, \\ 0 & \text{otherwise,} \end{cases} \quad J = \begin{cases} m & \text{for Cases I and II,} \\ k_2 & \text{for Case III,} \end{cases} \quad M = \begin{cases} m-1 & \text{for Case I,} \\ k_1 & \text{for Cases II and III,} \end{cases}$$

$$Q^\star = \begin{cases} n-m-\sum_{i=1}^{m-1} Q_i & \text{for Case I,} \\ n-m-\sum_{i=1}^{k_1} Q_i & \text{for Case II,} \\ n-k_2-\sum_{i=1}^{k_1} Q_i & \text{for Case III,} \end{cases} \quad \text{and } \tau = \begin{cases} x_m & \text{for Cases I and II,} \\ T_2 & \text{for Case III.} \end{cases}$$

In this context, $J_k = \sum_{i=1}^{J} I(\phi_i = r)$, for $r = 1, 2$, represents the number of observed failures attributed to cause r. Here, $I(\phi_i = r)$ is an indicator function that equals 1 if the i-th failure is due to cause r and 0 otherwise. The total number of observed failures, J, is the sum of failures from both causes, i.e., $J = J_1 + J_2$.

3. Classical point and interval estimations

In this section, the MLEs and the associated ACI for the BX parameters θ_r where $r = 1, 2$ are derived. Additionally, we compute the MLE and ACI for the RF. These derivations are carried out within the framework of the IAPT2C competing risks data, building on the assumptions outlined earlier. Consider an observed IAPT2C competing risks sample $\underline{\mathbf{x}}$, drawn from an BX population with the PDF and CDF given by (2.1) and (2.2), respectively. Using these, the likelihood function can be formulated on the basis of (2.4), without any constant term, as follows:

$$\begin{aligned} L(\boldsymbol{\theta}|\underline{\mathbf{x}}) &= \left(\prod_{r=1}^{2} \theta_r^{J_r}\right) \exp\left\{ \sum_{r=1}^{2} \sum_{i=1}^{J_r} \left[(\theta_r - 1)\log(y_i) + \log(1 - y_i^{\theta_{3-r}})\right] \right. \\ &+ \left. \sum_{r=1}^{2} \sum_{i=1}^{M} Q_i \log(1 - y_i^{\theta_r}) + \sum_{r=1}^{2} Q^\star \log(1 - y_\tau^{\theta_r}) \right\}, \end{aligned} \tag{3.1}$$

where $y_i = 1 - e^{-x_i^2}$ and $y_\tau = 1 - e^{-\tau^2}$. The log-likelihood function, denoted by $l(\boldsymbol{\theta}|\underline{\mathbf{x}})$, corresponds to (3.1) as follows:

$$\begin{aligned} l(\boldsymbol{\theta}|\underline{\mathbf{x}}) &= \sum_{r=1}^{2} J_r \log(\theta_r) + \sum_{r=1}^{2} \sum_{i=1}^{J_r} \left[(\theta_r - 1)\log(y_i) + \log(1 - y_i^{\theta_{3-r}})\right] \\ &+ \sum_{r=1}^{2} \sum_{i=1}^{M} Q_i \log(1 - y_i^{\theta_r}) + \sum_{r=1}^{2} Q^\star \log(1 - y_\tau^{\theta_r}), \end{aligned} \tag{3.2}$$

By setting the first-order partial derivatives of (3.2) with respect to θ_r (for $r = 1, 2$) to zero, we get the normal equations which must be solved to get the MLEs of the model parameters, denoted as $\hat{\theta}_r$, for $k = 1, 2$. The normal equations to be solved are given as

$$\frac{\partial l(\boldsymbol{\theta}|\underline{\mathbf{x}})}{\partial \theta_1} = \frac{J_1}{\theta_1} + \sum_{i=1}^{J_1} \log(y_i) + \sum_{i=1}^{J_2} \vartheta(y_i; \theta_1) + \sum_{i=1}^{M} Q_i \vartheta(y_i; \theta_1) + Q^\star \vartheta(\tau; \theta_1) = 0, \tag{3.3}$$

and

$$\frac{\partial l(\boldsymbol{\theta}|\underline{\mathbf{x}})}{\partial \theta_2} = \frac{J_2}{\theta_2} + \sum_{i=1}^{J_2} \log(y_i) + \sum_{i=1}^{J_1} \vartheta(y_i; \theta_2) + \sum_{i=1}^{M} Q_i \vartheta(y_i; \theta_2) + Q^\star \vartheta(\tau; \theta_2) = 0, \tag{3.4}$$

where $\vartheta(y_i;\theta_r) = \frac{\log(y_i)}{1-y_i^{\theta_r}}$ and $\vartheta(\tau;\theta_r) = \frac{\log(\tau)}{1-\tau^{\theta_r}}$. From Eqs (3.3) and(3.4), it is obvious that the classical estimators cannot be represented in closed form. Accordingly, getting the MLEs necessitates the usage of numerical iterative approaches. One useful procedure is the Newton Raphson algorithm, which can be applied to compute the required MLEs $\hat{\theta}_r$ for $r = 1, 2$. This algorithm is used for its fast quadratic convergence when solving nonlinear likelihood equations in (3.3) and (3.4). It offers greater efficiency and precision than first-order methods like gradient descent.

By employing the invariance property of the MLEs, the MLE of the RF at a specific time t, denoted as $\hat{R}(t) \equiv \hat{R}(t;\hat{\boldsymbol{\theta}})$, can be derived. This is achieved by substituting the MLEs of the parameters θ_r (for $r = 1, 2$) into the expression for the RF given in (2.3). Therefore, the MLE of the RF can be expressed using (2.3) as follows:

$$R(t) = \prod_{r=1}^{2}\left[1 - y_t^{\hat{\theta}_r}\right],$$

where $y_t = 1 - e^{-t^2}$.

To construct interval sets for the model parameters θ_r (for $r = 1, 2$) as well as the RF, it is essential to first obtain the asymptotic variance-covariance matrix. This matrix is typically derived from the Fisher information matrix, which involves computing the expectation of complex expressions. However, due to the complexity of these calculations, we instead approximate the Fisher information matrix using the observed Fisher information matrix. This approximation enables us to estimate the required variances and covariances efficiently. The estimated variance-covariance matrix, denoted as $\boldsymbol{I}^{-1}(\hat{\boldsymbol{\theta}})$, can be computed as given below:

$$\begin{aligned}\boldsymbol{I}(\hat{\boldsymbol{\theta}}) &= \left[\begin{array}{cc} -\frac{\partial^2 l(\boldsymbol{\theta}|\underline{\mathbf{x}})}{\partial\theta_1^2} & 0 \\ 0 & -\frac{\partial^2 l(\boldsymbol{\theta}|\underline{\mathbf{x}})}{\partial\theta_2^2}\end{array}\right]^{-1}_{\boldsymbol{\theta}=\hat{\boldsymbol{\theta}}} \\ &= \left[\begin{array}{cc} \hat{\sigma}_1^2 & 0 \\ 0 & \hat{\sigma}_2^2\end{array}\right], \end{aligned} \tag{3.5}$$

where

$$\frac{\partial^2 l(\boldsymbol{\theta}|\underline{\mathbf{x}})}{\partial\theta_1^2} = -\frac{J_1}{\theta_1^2} - \sum_{i=1}^{J_2}\vartheta_1(y_i;\theta_1) - \sum_{i=1}^{M} Q_i\vartheta_1(y_i;\theta_1) - Q^{\star}\vartheta_1(\tau;\theta_1),$$

and

$$\frac{\partial^2 l(\boldsymbol{\theta}|\underline{\mathbf{x}})}{\partial\theta_2^2} = -\frac{J_2}{\theta_2^2} - \sum_{i=1}^{J_1}\vartheta_1(y_i;\theta_2) - \sum_{i=1}^{M} Q_i\vartheta_1(y_i;\theta_2) - Q^{\star}\vartheta_1(\tau;\theta_2),$$

where $\vartheta_1(y_i;\theta_r) = \frac{\log^2(y_i)y_i^{-\theta_r}}{(1-y_i^{\theta_r})^2}$ and $\vartheta_1(\tau;\theta_r) = \frac{\log^2(\tau)\tau^{-\theta_r}}{(1-\tau^{\theta_r})^2}$.

By employing the asymptotic normality of the acquired MLEs, one can use the asymptotic distribution of $\hat{\boldsymbol{\theta}}$, expressed as $\hat{\boldsymbol{\theta}} \sim N_2(\boldsymbol{\theta}, \boldsymbol{I}(\hat{\boldsymbol{\theta}}))$, to compute the $100(1-\alpha)\%$ ACI of θ_r, where $r = 1, 2$, as follows:

$$\left[\hat{\theta}_r - z_{\alpha/2}\hat{\sigma}_r,\ \hat{\theta}_r + z_{\alpha/2}\hat{\sigma}_r\right],\ r = 1, 2,$$

where $z_{\alpha/2}$ denotes the critical value from the standard normal distribution, corresponding to the significance level α.

To construct the associated ACI for $R(t)$, we begin by approximating the variance of $\hat{R}(t)$ using the delta method. This method relies on the asymptotic normality of the MLEs and offers a way to approximate the variance of $\hat{R}(t)$. Specifically, the variance of $\hat{R}(t)$ is approximated as follows:

$$\hat{\sigma}_R^2 \approx \begin{bmatrix} \hat{R}_1 & \hat{R}_2 \end{bmatrix} \begin{bmatrix} \hat{\sigma}_1^2 & 0 \\ 0 & \hat{\sigma}_2^2 \end{bmatrix} \begin{bmatrix} \hat{R}_1 \\ \hat{R}_2 \end{bmatrix}, \tag{3.6}$$

where $\hat{R}_1 = -y_t^{\hat{\theta}_1} \log(y_t)(1 - y_t^{\hat{\theta}_2})$ and $\hat{R}_2 = -y_t^{\hat{\theta}_2} \log(y_t)(1 - y_t^{\hat{\theta}_1})$.

After computing the approximate variance of $\hat{R}(t)$, the $100(1-\alpha)\%$ ACI for $R(t)$ can be calculated as

$$\left[\hat{R}(t) - z_{\alpha/2}\,\hat{\sigma}_R,\ \hat{R}(t) + z_{\alpha/2}\,\hat{\sigma}_R\right].$$

4. Bayesian estimation

In this section, we explore the Bayesian estimation approach used to derive Bayes point estimates for the unknown parameters and the RF using both the SE and LINEX loss functions. Additionally, we construct the BCIs for these estimates. The computations are performed using the MCMC technique, which involves sampling from the posterior distribution.

In Bayesian analysis, the process begins by specifying prior distributions for the parameters. From the likelihood function provided in (3.1), it is clear that conjugate priors are not available for $\theta_r, r = 1, 2$. To address this, we adopt gamma priors, which are a suitable choice due to their flexibility in accommodating the range of unknown parameters while maintaining computational simplicity. Gamma priors are versatile and can effectively incorporate prior knowledge. Moreover, their use does not complicate the posterior evaluation or computational procedures, especially when employing the MCMC method.

Let $\theta_r \sim Gamma(\nu_r, \omega_r)$, where $\nu_r, \omega_r > 0$ and $r = 1, 2$. Here, the hyper-parameters ν_r and ω_r are assumed to be known. The joint prior distribution of $\theta_r, r = 1, 2$ is then given by

$$\pi(\boldsymbol{\theta}) \propto \prod_{r=1}^{2} \theta_r^{\nu_r - 1} e^{-\omega_r \theta_r}, \theta_r > 0, r = 1, 2. \tag{4.1}$$

By combining the likelihood function given in (3.1) with the joint prior distribution specified in (4.1), we can derive the joint posterior distribution of the model parameters $\boldsymbol{\theta}$. The posterior distribution represents the updated belief about the model parameters after incorporating the observed data and prior information. Mathematically, the joint posterior distribution can be expressed as follows:

$$\begin{aligned} \Psi(\boldsymbol{\theta}|\underline{\mathbf{x}}) &= A^{-1} \left(\prod_{r=1}^{2} \theta_r^{J_r + \nu_r - 1} \right) \exp\left\{ \sum_{r=1}^{2} \sum_{i=1}^{J_r} \left[\theta_r [\log(y_i) - \omega_r] + \log(1 - y_i^{\theta_{3-r}}) \right] \right. \\ &+ \left. \sum_{r=1}^{2} \sum_{i=1}^{M} Q_i \log(1 - y_i^{\theta_r}) + \sum_{r=1}^{2} Q^{\star} \log(1 - y_\tau^{\theta_r}) \right\}, \end{aligned} \tag{4.2}$$

where

$$A = \int_0^{\infty} \int_0^{\infty} \pi(\boldsymbol{\theta}) L(\boldsymbol{\theta}|\underline{\mathbf{x}}) d\theta_1 d\theta_2.$$

Let $\zeta(\boldsymbol{\theta})$ denote a parametric function of the unknown parameters $\boldsymbol{\theta}$. The Bayes estimator of $\zeta(\boldsymbol{\theta})$ is typically derived under a specific loss function. In this work, we consider two loss functions: The SE loss and the LINEX loss. It is worth noting that the Bayes estimator can also be obtained under other loss functions if desired. Under the SE loss function, the Bayes estimator of $\zeta(\boldsymbol{\theta})$, denoted as $\tilde{\zeta}(\boldsymbol{\theta})$, is defined as the posterior mean of $\zeta(\boldsymbol{\theta})$. Mathematically, it is expressed as the expected value of $\zeta(\boldsymbol{\theta})$ with respect to the posterior distribution of $\boldsymbol{\theta}$. Specifically, it is given by:

$$\tilde{\zeta}(\boldsymbol{\theta}) = \int_0^\infty \int_0^\infty \zeta(\boldsymbol{\theta})\pi(\boldsymbol{\theta})L(\boldsymbol{\theta}|\underline{\mathbf{x}})d\theta_1 d\theta_2. \tag{4.3}$$

On the other hand, under the LINEX loss function, the Bayes estimator of $\zeta(\boldsymbol{\theta})$ can be derived as follows:

$$\tilde{\tilde{\zeta}}(\boldsymbol{\theta}) = -\frac{1}{\delta}\log\left[\int_0^\infty \int_0^\infty e^{-\delta\zeta(\boldsymbol{\theta})}\pi(\boldsymbol{\theta})L(\boldsymbol{\theta}|\underline{\mathbf{x}})d\theta_1 d\theta_2\right], \tag{4.4}$$

where $\delta \neq 0$ is a shape parameter that controls the asymmetry of the loss function. This estimator minimizes the expected LINEX loss and is especially valuable in scenarios where the consequences of overestimation and underestimation are not symmetric.

The Bayes estimators given in (4.3) and (4.4) involve the computation of highly complex integrals, which are analytically challenging to solve due to the intricate nature of the posterior distribution. To overcome this difficulty, we employ the MCMC method. This approach enables direct sampling from the posterior distribution specified in (4.2). The resulting samples are then utilized to approximate the Bayes estimators and construct Bayesian credible intervals (BCIs). A crucial step in applying the MCMC method is obtaining the full conditional distributions of the unknown parameters. Based on the joint posterior distribution presented in (4.2), the conditional distributions for the parameters θ_1 and θ_2 can be derived, respectively, as

$$\begin{aligned}\Psi_1(\theta_1|\theta_2,\underline{\mathbf{x}}) \;\propto\; & \theta_1^{J_1+\nu_1-1}\exp\left\{\theta_1\sum\nolimits_{i=1}^{J_1}[\log(y_i)-\omega_1] + \sum\nolimits_{i=1}^{J_2}\log(1-y_i^{\theta_1})\right. \\ & \left. + \sum\nolimits_{i=1}^{M} Q_i\log(1-y_i^{\theta_1}) + Q^\star\log(1-y_\tau^{\theta_1})\right\},\end{aligned} \tag{4.5}$$

and

$$\begin{aligned}\Psi_2(\theta_2|\theta_1,\underline{\mathbf{x}}) \;\propto\; & \theta_2^{J_2+\nu_2-1}\exp\left\{\theta_2\sum\nolimits_{i=1}^{J_2}[\log(y_i)-\omega_2] + \sum\nolimits_{i=1}^{J_1}\log(1-y_i^{\theta_2})\right. \\ & \left. + \sum\nolimits_{i=1}^{M} Q_i\log(1-y_i^{\theta_2}) + Q^\star\log(1-y_\tau^{\theta_2})\right\}.\end{aligned} \tag{4.6}$$

Upon examining the conditional distributions in (4.5) and (4.6), it becomes clear that these distributions cannot be reduced to any standard or well-known forms. As a result, direct sampling from these distributions is not feasible. To address this, we propose using the Metropolis-Hastings (M-H) algorithm, a widely used MCMC technique, to generate samples from these complex distributions. For the M-H algorithm, we adopt a normal distribution as the proposed distribution, which facilitates the sampling process. Once the required samples are generated, it becomes straightforward to compute the Bayes estimates using the SE and LINEX loss functions as well as the BCIs for the model parameters and the RF. The MCMC sampling procedure is given in Algorithm 1.

Algorithm 1 The MCMC sampling steps.

Input: Set $\theta_r^{(0)} = \hat{\theta}_r, r = 1, 2$

Input: Set $h = 1$

Output: Generate a sample $\theta_1^{(j)}$ from $\Psi_1(\theta_1|\theta_2, \underline{\mathbf{x}})$

Output: Draw a candidate value $\theta_1^{\star}$ from a normal distribution with a mean $\hat{\theta}_1$ and a variance $\hat{\sigma}_1^2$

Output: Calculate $\xi = \min\left[1, \frac{\Psi_1(\theta_1^{\star}|\theta_2^{(h-1)}, \underline{\mathbf{x}})}{\Psi_1(\theta_1^{(h-1)}|\theta_2^{(h-1)}, \underline{\mathbf{x}})}\right]$

Output: Generate a random number u using $U(0, 1)$

Accept $\theta_1^{\star}$

if $u \leq \xi$ **then**

  Set $\theta_1^{(h)} = \theta_1^{\star}$

  Otherwise set $\theta_1^{(h)} = \theta_1^{(h-1)}$

end if

Output: Generate $\theta_2^{(j)}$ from $\Psi_2(\theta_2|\theta_1, \underline{\mathbf{x}})$

Output: Calculate $R^{(h)} = \prod_{r=1}^{2}\left[1 - y_t^{\theta_r^{(h)}}\right]$

Input: Increase the iteration counter by updating h to $h + 1$

Input: Remove an initial portion of the iterations as the burn-in phase

Output: Find $\left[\theta_1^{(h)}, \theta_2^{(h)}, R^{(h)}\right], \quad h = 1, \ldots, \mathcal{B}$, where $\mathcal{B}$ denotes the number of iterations remaining after excluding the burn-in period

Input: Arrange $\left[\theta_1^{(h)}, \theta_2^{(h)}, R^{(h)}\right], \quad h = 1, \ldots, \mathcal{B}$ in ascending order

Output: Compute the Bayes estimates of $\theta_r, r = 1, 2$, and the RF under the SE loss as

$$\tilde{\theta}_r = \frac{1}{\mathcal{B}}\sum_{h=1}^{\mathcal{B}}\theta_r^{(h)}, r = 1, 2 \text{ and } \tilde{R} = \frac{1}{\mathcal{B}}\sum_{h=1}^{\mathcal{B}}R^{(h)}$$

Output: Compute the Bayes estimates of $\theta_r, r = 1, 2$, and the RF under the LINEX loss as

$$\tilde{\tilde{\theta}}_r = -\frac{1}{\delta}\log\left[\frac{1}{\mathcal{B}}\sum_{h=1}^{\mathcal{B}}e^{-\delta\theta_r^{(h)}}\right], r = 1, 2 \text{ and } \tilde{\tilde{R}} = -\frac{1}{\delta}\log\left[\frac{1}{\mathcal{B}}\sum_{h=1}^{\mathcal{B}}e^{-\delta R^{(h)}}\right]$$

Input: Sort the samples for θ_1 as $\theta_1^{[1]} < \cdots < \theta_1^{[\mathcal{B}]}$, for θ_2 as $\theta_2^{[1]} < \cdots < \theta_2^{[\mathcal{B}]}$, and for the RF as $R^{[1]} < \cdots < R^{[\mathcal{B}]}$

Output: Compute the $100(1 - \alpha)\%$ BCIs of $\theta_r, r = 1, 2$, and the RF as

$$\left\{\theta_r^{[\alpha\mathcal{B}/2]}, \theta_r^{[(1-\alpha/2)\mathcal{B}]}\right\}, r = 1, 2,$$

and

$$\left\{R^{[\alpha\mathcal{B}/2]}, R^{[(1-\alpha/2)\mathcal{B}]}\right\}$$

5. Monte Carlo comparisons

To rigorously assess the effectiveness of the theoretical findings, including both point and interval estimation under the maximum likelihood and Bayesian frameworks, several Monte Carlo simulation experiments are conducted. Assigning the true parameter values set as $(\theta_1, \theta_2,) = (0.5, 1.5)$, we generate 1000 independent IAPT2C competing risks, assuming that the underlying failure times follow a BX distribution. Additionally, all experimental setups are conducted across multiple setup configurations, including different values of n (total units under test), m (observed failures), $\mathbf{Q}$ (removal pattern), and threshold points $T_i, i = 1, 2$; see Table 1. Specifically, for each group of n, m, and $\mathbf{Q}$, we set $T_1 \in \{0.2, 0.3\}$, and $T_2 \in \{0.3, 0.4\}$. All calculations are carried out for the survival function $R(t)$ when the true value is taken as 0.8993. In all calculations proposed here, without loss of generality, we used the suggested true values of the BX model as starting points. To simulate an IAPT2C competing risks dataset from the BX(θ_1, θ_2) distribution, we take the generation steps depicted in Algorithm 2.

Table 1. Different evaluation setups in the Monte Carlo simulations.

(n, m)	Design	$\mathbf{Q}$	(n, m)	Design	$\mathbf{Q}$
(20,10)	[1]	$(2^5, 0^5)$	(20,16)	[1]	$(2^2, 0^{14})$
	[2]	$(0^2, 2^5, 0^3)$		[2]	$(0^7, 2^2, 0^7)$
	[3]	$(0^5, 2^5)$		[3]	$(0^{14}, 2^2)$
(40,20)	[1]	$(2^{10}, 0^{20})$	(40,30)	[1]	$(2^5, 0^{25})$
	[2]	$(0^{10}, 2^{10}, 0^{10})$		[2]	$(0^{12}, 2^5, 0^{13})$
	[3]	$(0^{20}, 2^{10})$		[3]	$(0^{25}, 2^5)$
(80,40)	[1]	$(2^{20}, 0^{20})$	(80,60)	[1]	$(2^{10}, 0^{50})$
	[2]	$(0^{10}, 2^{20}, 0^{10})$		[2]	$(0^{25}, 2^{10}, 0^{25})$
	[3]	$(0^{20}, 2^{20})$		[3]	$(0^{50}, 2^{10})$

Algorithm 2 The IAPT2C generation steps.

1: **Input:** Specify the parameter values for $\theta_j,\ j = 1, 2$
2: **Output:** Draw $(\omega_1, \omega_2, \ldots, \omega_m)$ from a uniform (0,1) distribution
3: **Output:** Compute the transformed variables as $\upsilon_i = \omega_i^{\left(i+\sum_{j=m-i+1}^{m} R_j\right)^{-1}}, \quad i = 1, 2, \ldots, m$
4: **Input:** Set $U_i = 1 - \upsilon_m \upsilon_{m-1} \cdots \upsilon_{m-i+1}$ for $i = 1, 2, \ldots, m$
5: **Input:** Set $X_i = F^{-1}(U_i; \theta_j), \quad j = 1, 2, \quad i = 1, 2, \ldots, m$
6: **Input:** Determine k_1 at threshold time T_1
7: **Input:** Discard $X_i,\ i = k_1 + 2, \ldots, m$ for Cases II and III
8: **Output:** Generate $(X_{k_1+2}, \ldots, X_m)$ from a truncated BX distribution $\frac{f(x)}{[1-F(X_{k_1+1})]}$
9: **Output:** Assign the cause of failure as 1 or 2 for each sample point
10: **Output:** Collect an IAPT2C competing risks sample with size m (for Case-I and Case-II) or size k_2 (for Case-III)

Using each simulated dataset, the MLEs and their corresponding 95% ACIs of $\theta_r,\ r = 1, 2$ and $R(t)$ are computed. The Newton Raphson method, implemented via the 'maxLik' package in R, is recommended for estimating each unknown subject. To evaluate the Bayesian point and credible estimations of $\theta_r,\ r = 1, 2$ or $R(t)$, two informative prior sets of $(\nu_r, \omega_r),\ r = 1, 2$ for $\theta_r j = 1, 2$, are taken into account, namely:

- Prior-1: $(\nu_1, \nu_2) = (2.5, 7.5)$ and $\omega_r = 5,\ r = 1, 2$;
- Prior-2: $(\nu_1, \nu_2) = (5, 15)$ and $\omega_r = 10,\ r = 1, 2$.

To calculate the Bayesian estimates (against the SEL and LINEX (with $\delta(= -2, +2)$) functions) and their 95% BCIs, the M-H algorithm is employed to gather $\mathcal{B} = 12000$ iterations, excluding the first 2000 (burn-in). The "coda" package, as proposed by Plummer et al. [34], is recommended for posterior inference.

Numerically, the mean point estimate (MPE) of $\theta_r,\ r = 1, 2$ or $R(t)$ (say, ϵ,) is obtained as

$$\text{MPE}(\ddot{\epsilon}) = \frac{1}{1000}\sum_{j=1}^{1000} \ddot{\epsilon}^{[j]},$$

where $\ddot{\epsilon}^{[j]}$ represents the estimate of ϵ obtained at $j-$th sample.

Furthermore, the associated root mean square error (RMSE), average relative absolute bias (ARAB), average interval length (AIL), and coverage percentage (CP) of ϵ are obtained as:

$$\text{RMSE}(\ddot{\epsilon}) = \sqrt{\frac{1}{1000}\sum_{j=1}^{1000} \left(\ddot{\epsilon}^{[j]} - \epsilon\right)^2},$$

$$\text{ARAB}(\ddot{\epsilon}) = \frac{1}{1000}\sum_{j=1}^{1000} \epsilon^{-1}\left|\ddot{\epsilon}^{[j]} - \epsilon\right|,$$

$$\text{AIL}^{95\%}(\epsilon) = \frac{1}{1000}\sum_{j=1}^{1000} (\mathbb{U}_{\ddot{\epsilon}^{[j]}} - \mathbb{L}_{\ddot{\epsilon}^{[j]}}),$$

and

$$\text{CP}^{95\%}(\epsilon) = \frac{1}{1000}\sum_{j=1}^{1000} \mathcal{D}_{(\mathbb{L}_{\ddot{\epsilon}^{[j]}};\mathbb{U}_{\ddot{\epsilon}^{[j]}})}(\epsilon),$$

respectively, where $\mathcal{D}(\cdot)$ is the indicator and ($\mathbb{L}(\cdot)$,$\mathbb{U}(\cdot)$) denotes the estimated interval limits.

In Tables 2–4, the MPEs, RMSEs, and ARABs of each parameters are reported in the first, second, and third columns, respectively. In Tables 5–7, the AILs and CP of each parameters are listed in the first and second columns, respectively. In the Supplementary File, for brevity, the full point estimation results of $\theta_r,\ r = 1, 2$ and $R(t)$ are presented.

Table 2. The point estimation results of θ_1.

n	m	Design	MLE	Symmetrical Bayes			Asymmetrical Bayes					
							$\delta = -2$			$\delta = +2$		
							Prior-1					
							Prior-2					
$(T_1, T_2) = (0.2, 0.3)$												
20	10	[1]	0.542	0.596	1.191	0.853	0.596	0.885	1.096	0.304	0.567	0.699	0.288	0.513
						0.440	0.517	0.798	0.461	0.242	0.408	0.418	0.151	0.225
		[2]	0.528	0.691	1.541	0.734	0.665	1.147	1.170	0.431	0.836	0.643	0.418	0.783
						0.763	0.574	0.988	0.783	0.343	0.686	0.742	0.270	0.396
		[3]	0.528	0.647	1.241	0.596	0.665	1.025	1.170	0.343	0.587	0.796	0.308	0.537
						0.763	0.542	0.929	0.783	0.246	0.484	0.742	0.242	0.362
	16	[1]	0.503	0.232	0.440	0.440	0.185	0.435	0.461	0.174	0.343	0.418	0.160	0.325
						0.885	0.186	0.388	0.918	0.162	0.312	0.843	0.144	0.215
		[2]	0.505	0.264	0.518	0.377	0.242	0.479	0.408	0.210	0.394	0.350	0.164	0.325
						0.453	0.242	0.414	0.466	0.170	0.325	0.440	0.147	0.225
		[3]	0.505	0.277	0.790	0.377	0.242	0.543	0.408	0.221	0.414	0.350	0.167	0.333
						0.453	0.252	0.483	0.466	0.176	0.375	0.440	0.150	0.234
$(T_1, T_2) = (0.3, 0.4)$														
20	10	[1]	0.622	0.412	0.646	0.437	0.335	0.612	0.445	0.285	0.514	0.430	0.275	0.484
						0.387	0.323	0.569	0.393	0.246	0.439	0.381	0.220	0.320
		[2]	0.655	0.650	0.723	0.755	0.371	0.687	0.768	0.324	0.613	0.741	0.320	0.576
						0.637	0.362	0.647	0.659	0.306	0.534	0.615	0.268	0.384
		[3]	0.635	0.469	0.669	0.786	0.347	0.631	0.800	0.293	0.533	0.772	0.285	0.500
						0.663	0.335	0.585	0.688	0.267	0.451	0.640	0.233	0.336
	16	[1]	0.635	0.220	0.421	0.844	0.211	0.408	0.861	0.202	0.318	0.823	0.197	0.315
						0.787	0.204	0.394	0.806	0.160	0.305	0.767	0.140	0.279
		[2]	0.623	0.353	0.536	0.805	0.280	0.514	0.823	0.241	0.418	0.785	0.221	0.376
						0.738	0.268	0.481	0.757	0.189	0.313	0.720	0.142	0.283
		[3]	0.621	0.388	0.601	0.815	0.311	0.574	0.834	0.272	0.429	0.793	0.226	0.408
						0.746	0.301	0.543	0.766	0.214	0.358	0.726	0.204	0.310

Table 3. The point estimation results of θ_2.

n	m	Design	MLE	Symmetrical Bayes			Asymmetrical Bayes					
							$\delta = -2$			$\delta = +2$		
							Prior-1					
							Prior-2					
$(T_1, T_2) = (0.2, 0.3)$												
20	10	[1]	1.877	1.208	0.589	1.284	0.797	0.493	1.372	0.704	0.479	1.185	0.698	0.441
						1.372	0.723	0.482	1.425	0.648	0.430	1.311	0.613	0.408
		[2]	1.662	1.242	0.596	1.519	0.846	0.564	1.598	0.824	0.525	1.425	0.813	0.511
						1.631	0.841	0.532	1.673	0.807	0.506	1.581	0.785	0.418
		[3]	1.675	1.287	0.714	1.519	0.884	0.578	1.598	0.845	0.549	1.425	0.824	0.543
						1.631	0.879	0.562	1.673	0.815	0.523	1.581	0.807	0.506
	16	[1]	1.550	1.039	0.483	1.372	0.709	0.453	1.425	0.602	0.382	1.311	0.502	0.327
						1.982	0.648	0.422	2.006	0.491	0.319	1.957	0.486	0.303
		[2]	1.594	1.165	0.574	2.260	0.770	0.478	2.324	0.688	0.459	2.180	0.684	0.436
						1.832	0.714	0.476	1.852	0.614	0.425	1.811	0.607	0.404
		[3]	1.566	1.125	0.529	2.260	0.717	0.465	2.324	0.637	0.412	2.180	0.508	0.337
						1.832	0.682	0.438	1.852	0.557	0.334	1.811	0.501	0.321
$(T_1, T_2) = (0.3, 0.4)$														
20	10	[1]	2.695	1.153	1.139	1.004	0.762	0.508	1.062	0.730	0.486	0.952	0.709	0.472
						0.915	0.756	0.492	1.041	0.704	0.452	0.817	0.607	0.402
		[2]	2.737	1.215	1.219	1.106	0.799	0.533	1.174	0.769	0.512	1.043	0.735	0.490
						0.984	0.795	0.523	1.096	0.724	0.462	0.894	0.642	0.427
		[3]	3.221	1.259	1.275	1.085	0.853	0.568	1.156	0.816	0.543	1.020	0.779	0.519
						0.957	0.848	0.557	1.081	0.762	0.477	0.857	0.655	0.430
	16	[1]	2.054	0.933	0.955	0.985	0.698	0.456	1.009	0.611	0.406	0.959	0.555	0.361
						0.762	0.680	0.434	0.792	0.541	0.331	0.738	0.462	0.308
		[2]	2.543	1.066	1.087	1.062	0.744	0.472	1.095	0.705	0.449	1.026	0.696	0.443
						0.827	0.729	0.470	0.864	0.638	0.424	0.799	0.587	0.390
		[3]	2.109	0.974	0.999	1.119	0.710	0.467	1.155	0.615	0.409	1.080	0.548	0.365
						0.871	0.700	0.444	0.902	0.539	0.343	0.846	0.491	0.328

Table 4. The point estimation results of $R(t)$.

n	m	Design	MLE	Symmetrical Bayes			Asymmetrical Bayes					
							$\delta = -2$			$\delta = +2$		
							Prior-1 Prior-2					
$(T_1, T_2) = (0.2, 0.3)$												
20	10	[1]	0.902	0.119	0.153	0.984	0.108	0.106	0.984	0.091	0.080	0.984	0.072	0.074
						0.962	0.101	0.100	0.962	0.063	0.071	0.961	0.038	0.050
		[2]	0.901	0.129	0.157	0.984	0.115	0.118	0.984	0.102	0.104	0.984	0.086	0.095
						0.962	0.104	0.112	0.962	0.074	0.082	0.961	0.040	0.058
		[3]	0.905	0.104	0.145	0.978	0.098	0.099	0.978	0.085	0.070	0.977	0.063	0.069
						0.831	0.091	0.094	0.845	0.061	0.067	0.814	0.037	0.046
	16	[1]	0.900	0.096	0.133	0.773	0.089	0.095	0.792	0.080	0.085	0.752	0.061	0.063
						0.857	0.084	0.091	0.863	0.055	0.061	0.850	0.035	0.043
		[2]	0.900	0.087	0.126	0.773	0.084	0.090	0.792	0.069	0.072	0.752	0.051	0.054
						0.857	0.079	0.088	0.863	0.050	0.053	0.850	0.032	0.040
		[3]	0.899	0.082	0.114	0.831	0.078	0.087	0.845	0.055	0.061	0.814	0.050	0.054
						0.972	0.069	0.072	0.973	0.047	0.050	0.971	0.030	0.039
$(T_1, T_2) = (0.3, 0.4)$														
20	10	[1]	0.907	0.097	0.118	0.958	0.085	0.111	0.959	0.059	0.068	0.957	0.057	0.063
						0.918	0.076	0.088	0.919	0.057	0.060	0.917	0.053	0.048
		[2]	0.904	0.109	0.126	0.952	0.111	0.119	0.953	0.085	0.071	0.951	0.062	0.069
						0.907	0.104	0.115	0.908	0.061	0.068	0.906	0.055	0.055
		[3]	0.912	0.087	0.110	0.843	0.076	0.102	0.846	0.053	0.062	0.838	0.047	0.058
						0.792	0.065	0.079	0.796	0.043	0.058	0.789	0.043	0.043
	16	[1]	0.907	0.076	0.093	0.959	0.071	0.083	0.960	0.052	0.055	0.959	0.044	0.049
						0.932	0.061	0.072	0.933	0.038	0.053	0.932	0.037	0.040
		[2]	0.910	0.073	0.083	0.961	0.066	0.076	0.962	0.051	0.051	0.960	0.041	0.044
						0.937	0.058	0.068	0.938	0.036	0.049	0.937	0.035	0.039
		[3]	0.913	0.065	0.077	0.960	0.061	0.071	0.961	0.048	0.046	0.960	0.040	0.040
						0.931	0.054	0.062	0.931	0.034	0.044	0.930	0.033	0.036

Table 5. The 95% interval estimation results of θ_1.

n	m	Design	ACI		BCI				ACI		BCI			
					Prior-1		Prior-2				Prior-1		Prior-2	
			$(T_1, T_2) = (0.2, 0.3)$						$(T_1, T_2) = (0.3, 0.4)$					
20	10	[1]	0.829	0.933	0.782	0.938	0.614	0.941	0.726	0.934	0.543	0.944	0.497	0.943
		[2]	1.070	0.929	0.903	0.932	0.679	0.938	0.888	0.931	0.635	0.940	0.524	0.942
		[3]	0.926	0.931	0.833	0.935	0.654	0.939	0.789	0.933	0.597	0.942	0.505	0.943
	16	[1]	0.685	0.939	0.535	0.944	0.520	0.945	0.519	0.940	0.503	0.946	0.421	0.946
		[2]	0.728	0.937	0.626	0.942	0.548	0.944	0.587	0.939	0.513	0.946	0.438	0.946
		[3]	0.788	0.936	0.686	0.941	0.584	0.942	0.641	0.936	0.527	0.945	0.478	0.944
40	20	[1]	0.570	0.943	0.412	0.946	0.398	0.951	0.410	0.944	0.387	0.948	0.353	0.952
		[2]	0.631	0.940	0.489	0.945	0.475	0.947	0.485	0.941	0.460	0.947	0.411	0.948
		[3]	0.618	0.941	0.459	0.945	0.435	0.949	0.442	0.943	0.412	0.947	0.405	0.950
	30	[1]	0.457	0.946	0.330	0.948	0.312	0.954	0.358	0.948	0.340	0.950	0.288	0.956
		[2]	0.493	0.945	0.352	0.947	0.325	0.954	0.388	0.947	0.361	0.949	0.291	0.956
		[3]	0.524	0.944	0.387	0.947	0.379	0.952	0.390	0.946	0.373	0.949	0.310	0.954
80	40	[1]	0.364	0.949	0.263	0.951	0.252	0.956	0.275	0.951	0.255	0.953	0.236	0.957
		[2]	0.429	0.946	0.298	0.949	0.286	0.955	0.313	0.948	0.310	0.951	0.271	0.957
		[3]	0.405	0.947	0.289	0.950	0.275	0.955	0.284	0.949	0.275	0.952	0.269	0.957
	60	[1]	0.258	0.952	0.214	0.954	0.199	0.959	0.225	0.953	0.207	0.955	0.185	0.960
		[2]	0.277	0.952	0.226	0.954	0.215	0.958	0.268	0.952	0.213	0.954	0.209	0.958
		[3]	0.292	0.951	0.239	0.953	0.225	0.958	0.273	0.951	0.233	0.953	0.223	0.958

Table 6. The 95% interval estimation results of θ_2.

n	m	Design	ACI		BCI				ACI		BCI			
					Prior-1		Prior-2				Prior-1		Prior-2	
			$(T_1, T_2) = (0.2, 0.3)$						$(T_1, T_2) = (0.3, 0.4)$					
20	10	[1]	1.714	0.883	1.237	0.907	0.892	0.915	1.534	0.891	1.136	0.909	0.782	0.917
		[2]	1.789	0.881	1.375	0.904	0.966	0.911	1.593	0.885	1.244	0.906	0.845	0.913
		[3]	1.856	0.877	1.428	0.900	1.018	0.908	1.644	0.879	1.382	0.903	0.928	0.911
	16	[1]	1.453	0.905	0.920	0.912	0.716	0.918	1.366	0.907	0.743	0.914	0.714	0.920
		[2]	1.592	0.889	1.083	0.909	0.814	0.917	1.485	0.904	0.892	0.911	0.774	0.918
		[3]	1.533	0.902	0.977	0.911	0.783	0.918	1.408	0.906	0.828	0.912	0.759	0.919
40	20	[1]	1.276	0.912	0.782	0.918	0.636	0.922	0.946	0.915	0.678	0.920	0.615	0.923
		[2]	1.327	0.910	0.824	0.915	0.680	0.921	1.130	0.913	0.682	0.916	0.629	0.923
		[3]	1.409	0.907	0.880	0.914	0.698	0.920	1.317	0.910	0.707	0.915	0.672	0.922
	30	[1]	0.858	0.917	0.748	0.920	0.533	0.924	0.770	0.919	0.611	0.921	0.523	0.926
		[2]	1.088	0.913	0.774	0.919	0.587	0.924	0.889	0.916	0.628	0.921	0.570	0.925
		[3]	0.972	0.915	0.754	0.919	0.553	0.924	0.805	0.917	0.623	0.921	0.545	0.926
80	40	[1]	0.690	0.921	0.543	0.924	0.496	0.926	0.606	0.923	0.500	0.926	0.465	0.928
		[2]	0.717	0.920	0.694	0.921	0.508	0.925	0.674	0.922	0.527	0.923	0.484	0.927
		[3]	0.796	0.918	0.712	0.920	0.521	0.925	0.714	0.921	0.543	0.922	0.512	0.926
	60	[1]	0.557	0.925	0.436	0.928	0.419	0.929	0.505	0.926	0.425	0.928	0.412	0.930
		[2]	0.632	0.922	0.491	0.926	0.455	0.928	0.541	0.925	0.489	0.927	0.440	0.929
		[3]	0.580	0.924	0.484	0.926	0.436	0.929	0.529	0.926	0.476	0.928	0.432	0.930

Table 7. The 95% interval estimation results of $R(t)$.

n	m	Design	ACI		BCI				ACI		BCI			
					Prior-1		Prior-2				Prior-1		Prior-2	
			$(T_1, T_2) = (0.2, 0.3)$						$(T_1, T_2) = (0.3, 0.4)$					
20	10	[1]	0.323	0.933	0.211	0.936	0.201	0.938	0.237	0.852	0.192	0.937	0.179	0.939
		[2]	0.352	0.932	0.227	0.936	0.215	0.937	0.271	0.852	0.195	0.937	0.190	0.938
		[3]	0.296	0.935	0.198	0.937	0.191	0.938	0.215	0.816	0.189	0.938	0.168	0.940
	16	[1]	0.277	0.936	0.182	0.937	0.173	0.940	0.186	0.846	0.180	0.938	0.158	0.941
		[2]	0.229	0.938	0.171	0.938	0.157	0.941	0.178	0.831	0.178	0.938	0.145	0.942
		[3]	0.190	0.938	0.163	0.939	0.143	0.942	0.171	0.842	0.172	0.940	0.136	0.943
40	20	[1]	0.155	0.941	0.142	0.941	0.133	0.943	0.158	0.847	0.142	0.942	0.117	0.945
		[2]	0.174	0.940	0.154	0.940	0.139	0.943	0.164	0.868	0.153	0.941	0.124	0.944
		[3]	0.147	0.942	0.133	0.942	0.123	0.944	0.143	0.825	0.135	0.942	0.107	0.946
	30	[1]	0.136	0.942	0.122	0.943	0.119	0.945	0.133	0.859	0.131	0.942	0.101	0.946
		[2]	0.129	0.943	0.118	0.943	0.110	0.946	0.127	0.836	0.122	0.944	0.092	0.947
		[3]	0.120	0.944	0.107	0.944	0.103	0.946	0.112	0.875	0.116	0.945	0.090	0.947
80	40	[1]	0.102	0.945	0.091	0.946	0.088	0.948	0.098	0.836	0.098	0.947	0.073	0.949
		[2]	0.114	0.945	0.101	0.944	0.092	0.947	0.102	0.858	0.111	0.945	0.082	0.948
		[3]	0.094	0.946	0.088	0.946	0.081	0.948	0.090	0.810	0.089	0.947	0.069	0.949
	60	[1]	0.090	0.946	0.076	0.947	0.071	0.949	0.085	0.856	0.085	0.948	0.063	0.950
		[2]	0.088	0.947	0.071	0.947	0.065	0.949	0.082	0.817	0.073	0.948	0.059	0.951
		[3]	0.081	0.947	0.068	0.948	0.050	0.950	0.079	0.835	0.061	0.949	0.052	0.951

From Tables 2–7, in terms of the lowest RMSE, ARAB, and AIL values, as well as the highest CP values, several key insights regarding the estimation of $\theta_r,\ r = 1, 2$, and $R(t)$ are presented as follows.

- Overall, both point and interval estimates of $\theta_r,\ r = 1, 2$, and $R(t)$ developed from classical and Bayesian estimation approaches yield satisfactory results.
- As n (or m) increases, a decreasing trend is observed in RMSEs, ARABs, and AILs, while the corresponding CPs improve. A similar pattern emerges when the total of progressive removals, defined by $S_i,\ i = 1, 2, ..., m$, decreases.
- Bayesian estimation, both point and interval, exhibits superior performance compared with classical estimation, as it achieves lower RMSEs, ARABs, and AILs, alongside higher CPs. This advantage is expected since Bayesian methods incorporate prior knowledge about the parameters, leading to more precise inference.
- Increasing the threshold values $T_i,\ i = 1, 2$ generally results in reduced RMSEs and ARABs for all parameters. Concurrently, the AILs of ACI/BCI estimates were narrowed down, while their respective CPs increased. This behavior is intuitive, as larger threshold values allow for more informative data collection.
- Evaluating the impact of different designs of $\mathbf{Q}$, the simulation results indicate that both the classical and Bayesian estimators of $\theta_r,\ r = 1, 2$ perform optimally based on Design [1] while those of $R(t)$ perform adequately based on Design [3] for each group of (n, m).
- Bayesian estimation for each parameter based on Prior-2 demonstrates superior performance relative to estimates obtained using Prior-1. This enhanced precision arises from the fact that Prior-2 is associated with a smaller variance compared with Prior-1, thereby yielding more concentrated posterior distributions. Furthermore, both Bayesian priors outperform the classical approach, as Bayesian methods incorporate prior information, leading to improved estimation accuracy and reduced uncertainty.
- As a summary, the Bayesian estimation approach, particularly when implemented via the M-H algorithm, is recommended for estimating the unknown competing parameters and reliability index of the BX distribution when practitioners are interested in considering the IAPT2C competing risks framework.

6. Real applications

To show how the proposed methodology can be applied to real phenomena, we shall analyze two genuine real datasets collected from the veterinary radiology and electronic industry fields. Each data set consists of two causes of failure. Specifically, the first dataset consists of the lifetimes of male mice exposed to high levels of roentgen radiation, while the other contains the lifetimes of the electrodes after they were placed in a high-voltage stress test.

6.1. Veterinary radiology

Radiology veterinary techniques have significantly contributed to our understanding of tumor biology, transplant immunology, and the intricate mechanisms governing immune system responses. In this study, veterinary experimental data from a controlled laboratory investigation where male mice were subjected to a radiation dose of 300 roentgens are analyzed. The exposure occurred during a critical developmental period, specifically between 35 and 42 days of age (equivalent to five to

six weeks). Causes for this dataset are classified as "0" (censoring), "1" (cause of death due to reticulocyte sarcoma), or "2" (cause of death is other); see Kundu et al. [35] and Alotaibi et al. [36] for additional details. In Table 8, beyond dividing each male mouses's age by 500 (due to computational requirements), the new transformed radiation dataset is provided. In this application, by discarding any remaining lifespans, we only evaluate observations from causes 1 and 2 that are completely observed on the basis of competing risks.

To analyze the proposed estimation results, it is essential to evaluate whether the BX distribution adequately models the lifespan data of male mice (listed in Table 8). To achieve this, the MLE (with its standard error (Std.Er)) and 95% ACI (with its interval width (IW)) of BX(θ) and the Kolmogorov–Smirnov (KS) distance (with its P-value) are computed; see Table 9. It reveals that since the estimated P-value exceeds the preassigned significance level $\alpha = 5\%$, there is not sufficient statistical evidence to reject the assumption that the male mice's lifespans follow the BX distribution. Thus, the BX model provides an appropriate fit for the observed male mouse survival data gathered from each cause of death.

Table 8. Lifespans of male mice exposed to radiation.

Age [cause]									
0.634 [0]	0.636 [1]	0.798 [0]	0.990 [0]	1.050 [1]	1.072 [1]	1.098 [0]	1.104 [0]	1.108 [0]	1.114 [0]
1.116 [1]	1.142 [0]	1.172 [0]	1.188 [0]	1.192 [0]	1.210 [1]	1.224 [1]	1.242 [1]	1.256 [0]	1.262 [0]
1.272 [0]	1.286 [0]	1.294 [0]	1.296 [0]	1.298 [0]	1.322 [0]	1.326 [0]	1.332 [0]	1.340 [0]	1.390 [0]
1.394 [0]	1.400 [0]	1.410 [0]	1.424 [0]	1.426 [0]	1.476 [0]	1.496 [0]	1.506 [0]	0.080 [2]	0.084 [2]
0.102 [0]	0.124 [2]	0.326 [2]	0.358 [2]	0.412 [2]	0.444 [2]	0.456 [2]	0.504 [2]	0.518 [2]	0.564 [0]
0.648 [0]	0.666 [0]	0.682 [0]	0.732 [0]	0.770 [2]	0.814 [2]	0.840 [2]	0.862 [0]	0.882 [0]	0.922 [0]
0.924 [2]	0.964 [0]	1.034 [2]	1.034 [2]	1.048 [2]	1.128 [0]	1.134 [0]	1.172 [0]	1.238 [0]	1.240 [2]
1.242 [0]	1.244 [0]	1.294 [0]	1.302 [0]	1.372 [0]	1.522 [0]	1.526 [0]			

Table 9. Fitting results of the BX(θ) model from veterinary radiology data.

Cause	MLE (Std.Er)	95% ACI [IW]	KS (P-value)
Cause 1	1.3007 (0.4916)	(0.3371,2.2643) [1.9272]	0.3234 (0.3758)
Cause 2	0.5797 (0.1366)	(0.3119,0.8474) [0.5356]	0.1540 (0.7870)

Additionally, as a visual goodness-of-fit explanation, the empirical/estimated lines of $R(x)$, probability-probability (P-P), and log-likelihood lines are depicted in Figure 1. In Figure 1(a), the KS distance is represented by a solid red line. It demonstrates that the fitted RF (PP) lines match both veterinary radiology datasets' empirical RF (PP) lines. It also shows that the fitted values of $\hat{\theta}_r,\ r = 1, 2$ (reported in Table 9), exist and are unique. For the upcoming calculations developed from veterinary radiology data, we recommend utilizing $\hat{\theta}_1 \equiv 1.3007$ and $\hat{\theta}_2 \equiv 0.5797$ as the initial points for subsequent computational iterations.

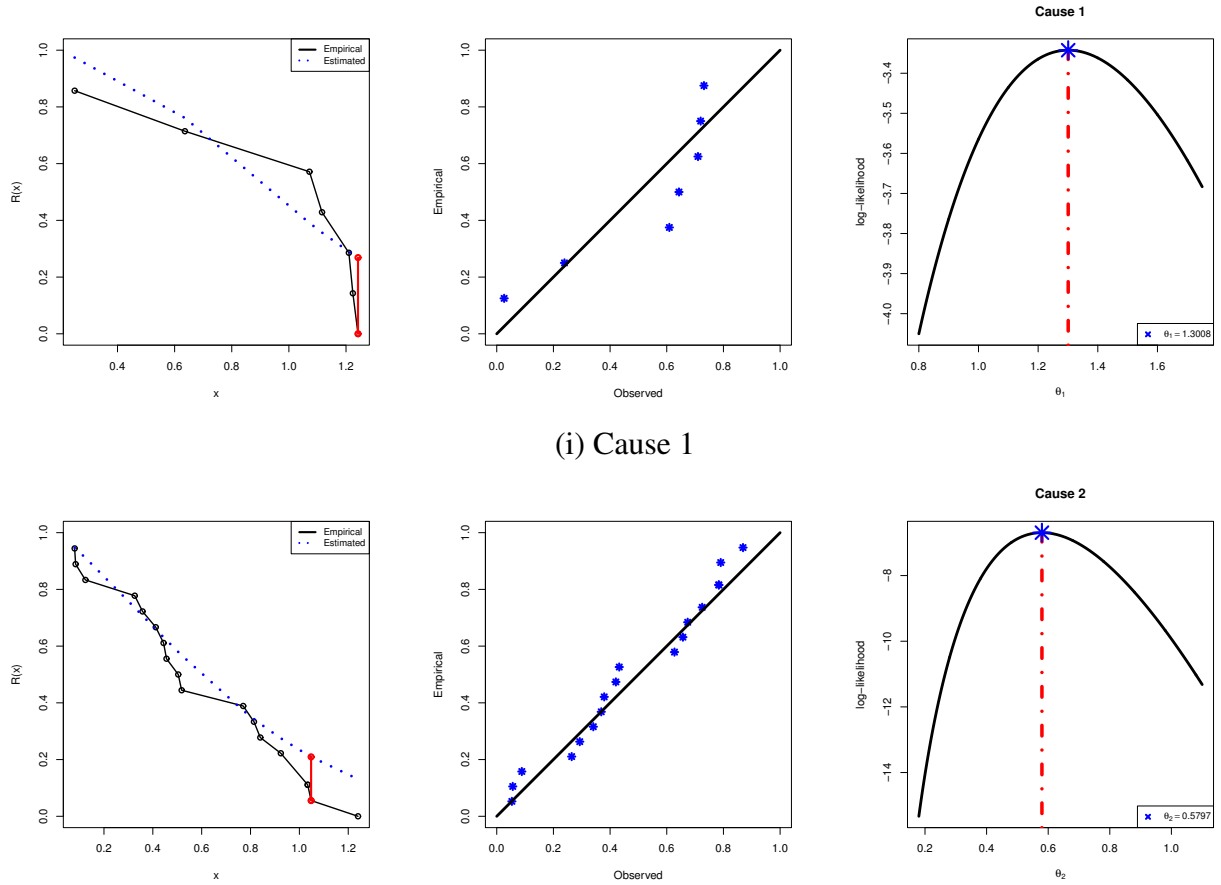

(i) Cause 1

(ii) Cause 2

(a) RF (b) PP (c) Profile

Figure 1. Three fitting diagrams of the BX(θ) model from the veterinary radiology data.

For a fixed $m = 15$ and various choices of T_i, $i = 1, 2$, and S_i, $i = 1, 2, ..., m$, three IAPT2C competing risk samples from the veterinary radiology data are generated; see Table 10. For each dataset in Table 10, both the point and interval estimates acquired from maximum likelihood and Bayesian methodologies are computed for θ_r, $r = 1, 2$, and $R(t)$ (at $t = 0.25$); see Tables 11–12. In the Bayesian estimation framework, due to the prior knowledge about the BX parameters θ_r, $r = 1, 2$, the hyper-parameters ν_r and ω_r (for $r = 1, 2$) are chosen as $\nu_r = \omega_r = 0.001$ to reflect non-informative priors. The M-H sampler, as detailed in Section 4, is employed to generate 50,000 MCMC samples, with the first 10,000 iterations discarded as burn-in.

The results in Tables 11–12 reveal that in terms of minimum Std.Er and IW values, the point and 95% interval estimates obtained with the Bayesian setup outperform those developed from the likelihood setup. Furthermore, when $\delta \to 0$, the asymmetrical Bayes estimates (developed from LINEX (for $\delta(= -3, -0.03, +3)$)) behave similarly to the symmetrical Bayes estimates (developed from SEL).

Table 10. Three IAPT2C competing risk samples from veterinary radiology data.

Sample	**Q**	T_1 (k_1)	T_2 (k_2)	τ	Failure [cause]					(J_1, J_2)	Q^*
$\mathbb{S}1$	$(2^5, 0^{10})$	0.35 (3)	1.23 (14)	1.23	0.080 [2]	0.124 [2]	0.326 [2]	0.358 [2]	0.412 [2]	(4,10)	5
					0.444 [2]	0.456 [2]	0.518 [2]	0.636 [1]	0.770 [2]		
					0.814 [2]	1.072 [1]	1.116 [1]	1.224 [1]			
$\mathbb{S}2$	$(0^5, 2^5, 0^5)$	0.45 (7)	0.93 (13)	0.93	0.080 [2]	0.084 [2]	0.124 [2]	0.250 [1]	0.326 [2]	(2,11)	8
					0.358 [2]	0.444 [2]	0.456 [2]	0.518 [2]	0.636 [1]		
					0.770 [2]	0.814 [2]	0.924 [2]				
$\mathbb{S}3$	$(0^{10}, 2^5)$	0.52 (11)	0.64 (12)	0.64	0.080 [2]	0.084 [2]	0.124 [2]	0.250 [1]	0.326 [2]	(2,10)	11
					0.358 [2]	0.412 [2]	0.444 [2]	0.456 [2]	0.504 [2]		
					0.518 [2]	0.636 [1]					

Table 11. Point estimates of $\theta_r,\ r = 1, 2$, and $R(t)$ from the veterinary radiology data.

Sample	Par.	MLE		SEL		LINEX					
		Est.	Std.Er	Est.	Std.Er	Est.	Std.Er	Est.	Std.Er	Est.	Std.Er
$\delta \rightarrow$						-3		-0.03		+3	
$\mathbb{S}1$	θ_1	0.8361	0.1383	0.5651	1.1071	0.5750	1.0462	0.5632	1.0794	0.5567	1.0274
	θ_2	7.5998	1.5853	4.4926	10.707	4.5713	10.1180	4.4769	10.4392	4.4252	9.9360
	$R(t)$	0.7168	0.0591	0.6010	0.8326	0.6115	0.7868	0.5989	0.8117	0.5919	0.7726
$\mathbb{S}2$	θ_1	0.7647	0.1154	0.5385	0.9910	0.5479	0.9365	0.5366	0.9662	0.5304	0.9196
	θ_2	7.9206	1.7123	4.5645	11.277	4.6444	10.656	4.5485	10.995	4.4960	10.465
	$R(t)$	0.6845	0.0549	0.5769	0.7922	0.5870	0.7486	0.5749	0.7724	0.5682	0.7352
$\mathbb{S}3$	θ_1	0.7223	0.1103	0.5061	0.9386	0.5149	0.8870	0.5043	0.9151	0.4985	0.8710
	θ_2	6.7740	1.4603	3.9119	9.6360	3.9803	9.1060	3.8982	9.3951	3.8532	8.9422
	$R(t)$	0.6637	0.0560	0.5540	0.7734	0.5637	0.7309	0.5520	0.7541	0.5457	0.7177

Table 12. Interval estimates of $\theta_r,\ r = 1, 2$ and $R(t)$ from veterinary radiology data.

Sample	Par.	ACI			BCI		
		Lower	Upper	IW	Lower	Upper	IW
$\mathbb{S}1$	θ_1	0.5420	0.8329	0.1135	0.6194	1.0629	0.4435
	θ_2	6.2143	7.5908	0.1986	7.1994	7.9799	0.7805
	$R(t)$	0.2316	0.7112	0.0493	0.6072	0.7988	0.1916
$\mathbb{S}2$	θ_1	0.4525	0.7615	0.0969	0.5799	0.9594	0.3795
	θ_2	6.7122	7.9124	0.1803	7.5635	8.2638	0.7003
	$R(t)$	0.2153	0.6796	0.0467	0.5831	0.7648	0.1817
$\mathbb{S}3$	θ_1	0.4325	0.7197	0.0940	0.5439	0.9127	0.3687
	θ_2	5.7242	6.7674	0.1794	6.4150	7.1198	0.7048
	$R(t)$	0.2194	0.6589	0.0482	0.5598	0.7476	0.1878

To evaluate the convergence behavior and mixing efficiency of the MCMC process, from Table 10, both the density (with Gaussian curve) and trace plots of θ_r, $r = 1, 2$, and $R(t)$ based on their remaining 40,000 MCMC variates are plotted in Figure 2. These visual diagnostics are presented in Figure 2. It indicates that the posterior distributions of θ_1, θ_2, and $R(t)$ exhibit near symmetry, positively skewed, and negatively skewed, respectively. It also exhibits that the collected Markovian iterations for all unknown quantities are effective mixing, confirming the stability and reliability of the Bayesian inference.

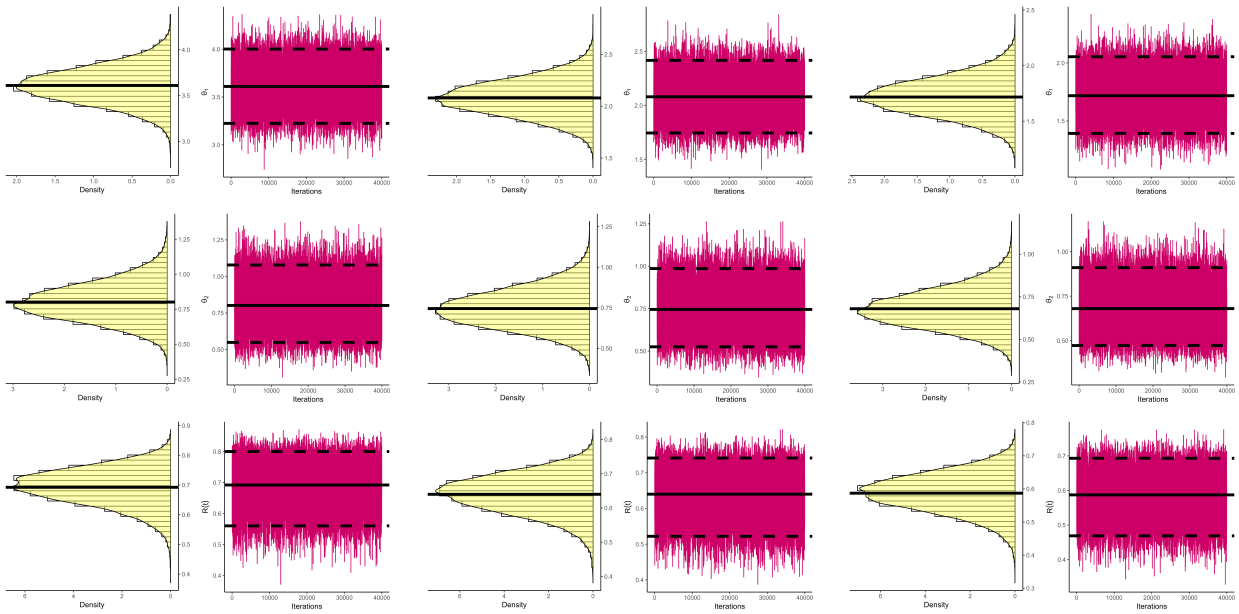

(a) Sample $\mathbb{S}1$ (b) Sample $\mathbb{S}2$ (c) Sample $\mathbb{S}3$

Figure 2. Density (left) and trace (right) plots from the veterinary radiology data.

6.2. Electronic industry

Electrodes extracted as segmented parts from conductor bars are typically subjected to high-voltage life testing to evaluate their electrical durability and failure characteristics under severe operating conditions. This experimental setup aims to assess the longevity and degradation mechanisms of the electrode material when exposed to sustained high-voltage stress. In this application, we are interested in examining 58 electrodes (cut-off parts of bars) that have been subjected to a high voltage resistance test. Electrode failures (in 200 hours) are recorded according to the technical causes of failure, namely 0 (electrodes were still running), 1 (insulation defect due to processing problem), and 2 (organic material deterioration); see Table 13. Recently, this dataset has been reanalyzed by Elshahhat and Nassar [24] and Alqasem et al. [37].

For this analysis, we focus exclusively on fully observed failure times from the electrode dataset, omitting right-censored observations (denoted as 0), which correspond to units that remain operational. To assess the suitability of the BX distribution in modeling the lifespan data of the electrodes, besides the KS (with its P-value), we compute the MLE (with its Std.Er) and 95% ACI (with its IW) of the BX(θ) model; see Table 14. The statistical findings (presented in Table 14) support the BX model as a reliable representation of the observed electrodes data set, stratified by cause of failure. Additionally,

the fitting facts shown in Figure 3 support the same fact reported in Table 3.

Table 13. Lifespans of 58 electrodes.

Observation [cause]							
0.010 [1]	0.015 [1]	0.025 [1]	0.040 [1]	0.065 [0]	0.105 [1]	0.140 [1]	0.155 [1]
0.155 [0]	0.260 [0]	0.265 [0]	0.320 [1]	0.335 [0]	0.345 [1]	0.380 [1]	0.390 [0]
0.520 [1]	0.565 [0]	0.595 [1]	0.675 [0]	0.720 [1]	0.785 [0]	0.800 [1]	0.840 [2]
0.895 [0]	0.955 [2]	1.015 [2]	1.055 [2]	1.105 [1]	1.130 [1]	1.180 [1]	1.205 [0]
1.285 [0]	1.305 [2]	1.320 [2]	1.390 [2]	1.410 [1]	1.420 [2]	1.430 [2]	1.490 [2]
1.515 [1]	1.570 [2]	1.585 [2]	1.590 [2]	1.600 [2]	1.635 [2]	1.640 [2]	1.640 [2]
1.740 [2]	1.740 [0]	1.750 [2]	1.800 [2]	1.845 [2]	1.885 [2]	1.935 [2]	1.960 [2]
2.060 [2]	2.230 [2]						

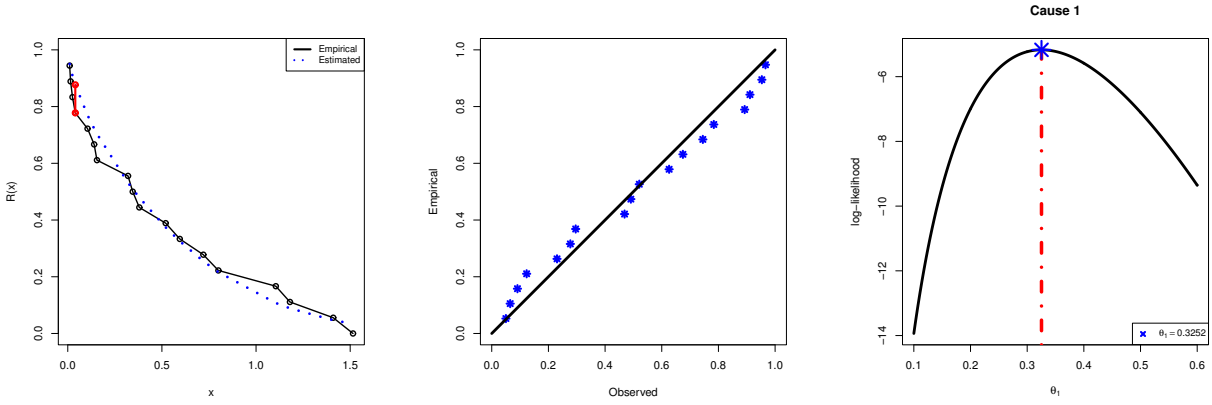

(i) Cause 1

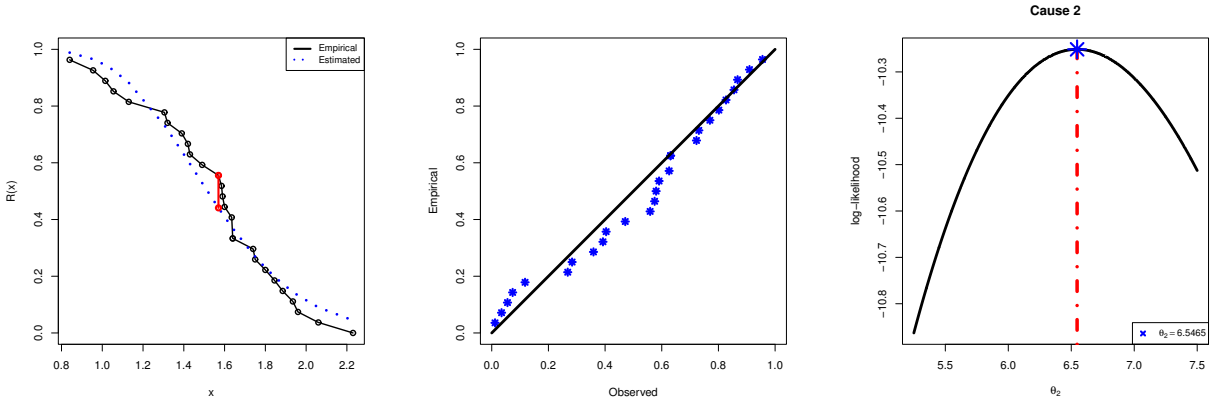

(ii) Cause 2

(a) RF (b) PP (c) Profile

Figure 3. Three fitting diagrams of the BX(θ) model from the electrode data.

Table 14. Fitting results of the BX(θ) model from the electrode data.

Cause	MLE (Std.Er)	95% ACI [IW]	KS (P-value)
Cause 1	0.3252 (0.0767)	(0.1750,0.4755) [0.3005]	0.1148 (0.9500)
Cause 2	6.5465 (1.2599)	(4.0772,9.0158) [4.9385]	0.1516 (0.5645)

Taking $m = 25$, three IAPT2C competing risk samples from electrodes data are generated using different configurations of T_i, $i = 1, 2$, and Q_i, $i = 1, 2, \ldots, m$; see Table 15. For each dataset, point and interval estimates of the BX model parameters θ_r, $r = 1, 2$, and $R(t)$ (when $t = 0.25$) are computed using both maximum likelihood and Bayesian inferences; see Tables 16–17. In this application, we follow the same Bayes evaluations implemented in Subsection 6.1 to carry out the point MCMC estimates from the SEL and LINEX (for $\delta(= -3, -0.03, +3)$) functions and to carry out the credible interval estimates.

The estimation results in Tables 16–17 indicate that, in terms of lower Std.Ers and narrower IWs, the Bayesian estimates of θ_r, $r = 1, 2$, and $R(t)$ provide superior accuracy compared with their likelihood-based counterparts. Furthermore, Table 16 indicates that the asymmetric Bayes estimates derived from the LINEX loss exhibit behavior similar to the symmetric Bayes estimates obtained using the SEL at δ near to zero. Moreover, Table 16 indicates that the estimates created by the LINEX loss (when $\delta < 0$) are overestimates, while those created by the LINEX loss (when $\delta > 0$) are underestimates.

Table 15. Three IAPT2C competing risk samples from the electrode data.

Sample	**Q**	T_1 (k_1)	T_2 (k_2)	τ	Failure [cause]					(J_1, J_2)	Q^*
$\mathbb{S}1$	$(2^{10}, 0^{15})$	0.35 (6)	1.65 (24)	1.65	0.010[1]	0.025 [1]	0.040 [1]	0.105 [1]	0.155 [1]	(15,9)	9
					0.345 [1]	0.380 [1]	0.595 [1]	0.720 [1]	0.800 [1]		
					0.840 [2]	0.955 [2]	1.015 [2]	1.105 [1]	1.130 [1]		
					1.180 [1]	1.320 [2]	1.390 [2]	1.410 [1]	1.490 [2]		
					1.515 [1]	1.570 [2]	1.590 [2]	1.640 [2]			
$\mathbb{S}2$	$(0^7, 2^{10}, 0^8)$	0.82 (12)	1.60 (22)	1.60	0.010 [1]	0.015 [1]	0.025 [1]	0.040 [1]	0.105 [1]	(15,7)	13
					0.140 [1]	0.155 [1]	0.320 [1]	0.380 [1]	0.595 [1]		
					0.720 [1]	0.800 [1]	0.840 [2]	0.955 [2]	1.015 [2]		
					1.105 [1]	1.180 [1]	1.320 [2]	1.390 [2]	1.410 [1]		
					1.490 [2]	1.570 [2]					
$\mathbb{S}3$	$(0^{15}, 2^{10})$	1.15 (19)	1.20 (20)	1.20	0.010 [1]	0.015 [1]	0.025 [1]	0.040 [1]	0.105 [1]	(17,3)	17
					0.140 [1]	0.155 [1]	0.320 [1]	0.345 [1]	0.380 [1]		
					0.520 [1]	0.595 [1]	0.720 [1]	0.800 [1]	0.840 [2]		
					0.955 [2]	1.015 [2]	1.105 [1]	1.130 [1]	1.180 [1]		

Table 16. Point estimates of $\theta_r,\ r = 1, 2$, and $R(t)$ from the electrode data.

Sample	Par.	MLE		SEL		LINEX					
		Est.	Std.Er	Est.	Std.Er	Est.	Std.Er	Est.	Std.Er	Est.	Std.Er
$\delta \rightarrow$						-3		-0.03		+3	
$\mathbb{S}1$	θ_1	0.8361	0.1383	0.5651	1.1071	0.5750	1.0462	0.5632	1.0794	0.5567	1.0274
	θ_2	7.5998	1.5853	4.4926	10.7069	4.5713	10.1180	4.4769	10.4392	4.4252	9.9360
	$R(t)$	0.7168	0.0591	0.6010	0.8326	0.6115	0.7868	0.5989	0.8117	0.5919	0.7726
$\mathbb{S}2$	θ_1	0.7647	0.1154	0.5385	0.9910	0.5479	0.9365	0.5366	0.9662	0.5304	0.9196
	θ_2	7.9206	1.7123	4.5645	11.2767	4.6444	10.656	4.5485	10.995	4.4960	10.465
	$R(t)$	0.6845	0.0549	0.5769	0.7922	0.5870	0.7486	0.5749	0.7724	0.5682	0.7352
$\mathbb{S}2$	θ_1	0.7223	0.1103	0.5061	0.9386	0.5149	0.8870	0.5043	0.9151	0.4985	0.8710
	θ_2	6.7740	1.4603	3.9119	9.6360	3.9803	9.1060	3.8982	9.3951	3.8532	8.9422
	$R(t)$	0.6637	0.0560	0.5540	0.7734	0.5637	0.7309	0.5520	0.7541	0.5457	0.7177

Table 17. Interval estimates of $\theta_r,\ r = 1, 2$ and $R(t)$ from electrodes data.

Sample	Par.	ACI			BCI		
		Lower	Upper	IW	Lower	Upper	IW
$\mathbb{S}1$	θ_1	0.5420	0.8329	0.1135	0.6194	1.0629	0.4435
	θ_2	6.2143	7.5908	0.1986	7.1994	7.9799	0.7805
	$R(t)$	0.2316	0.7112	0.0493	0.6072	0.7988	0.1916
$\mathbb{S}2$	θ_1	0.4525	0.7615	0.0969	0.5799	0.9594	0.3795
	θ_2	6.7122	7.9124	0.1803	7.5635	8.2638	0.7003
	$R(t)$	0.2153	0.6796	0.0467	0.5831	0.7648	0.1817
$\mathbb{S}2$	θ_1	0.4325	0.7197	0.0940	0.5439	0.9127	0.3687
	θ_2	5.7242	6.7674	0.1794	6.4150	7.1198	0.7048
	$R(t)$	0.2194	0.6589	0.0482	0.5598	0.7476	0.1878

The graphical diagrams in Figure 4 reveal that the posterior distributions of θ_1 and $R(t)$ exhibit positive and negative skewness, respectively, while the posterior of θ_2 is near symmetry. Moreover, the MCMC trace plots indicate effective mixing of the Markovian iterates, ensuring the stability and efficiency of the Bayesian inference.

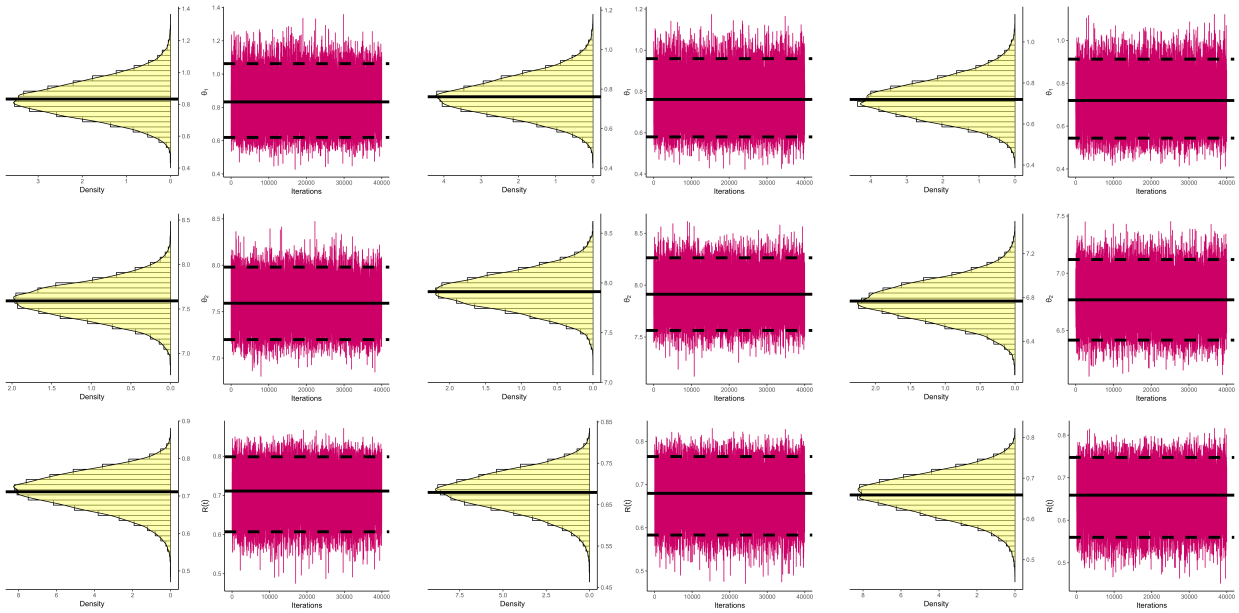

(a) Sample $\mathbb{S}1$ (b) Sample $\mathbb{S}2$ (c) Sample $\mathbb{S}3$

Figure 4. Density (left) and trace (right) plots from the electrode data.

7. Conclusions

This study addressed the challenges associated with analyzing competing risk data under the improved adaptive progressive Type-II censoring scheme, particularly in scenarios where test duration was a critical factor. By assuming independent Burr-X distributions for the lifetimes associated with competing risks, we developed both classical and Bayesian estimation methods to estimate the model parameters and the reliability function. The complexity of obtaining classical maximum likelihood estimates arose from the nonlinear nature of the likelihood equations, which did not yield closed-form solutions. To address this issue, the Newton Raphson method was employed to numerically solve the system of equations. The approximate confidence intervals derived from the asymptotic properties of the classical estimates provided a practical framework for inference, although their accuracy was contingent upon the sample size. On the Bayesian front, the complexity of the posterior distribution presented significant challenges in obtaining closed-form solutions for the Bayes estimates. To overcome this obstacle, we employed Markov chain Monte Carlo techniques, which facilitated sampling from the posterior distribution even when its form was analytically intractable. The Markov chain Monte Carlo approach, combined with the Metropolis-Hastings algorithm, enabled efficient generation of samples and computation of Bayes estimates under both squared error and linear exponential loss functions. Additionally, Bayesian credible intervals were constructed to quantify the uncertainty in the estimates. Through extensive simulation studies and real data analysis, the proposed methods demonstrated their effectiveness and applicability in reliability analyses. Monte Carlo simulations also showed that the predefined threshold values T_1 and T_2 significantly influence the estimation of any parametric function associated with the unknown parameters, highlighting their critical role in statistical modeling. The findings based on the radiation and electrodes data sets

reinforce the applicability of the proposed estimation methods to real-world reliability analysis. The results underscored the importance of the improved adaptive progressive Type-II censoring scheme and the Burr-X distribution in modeling competing risk data, providing valuable tools for reliability practitioners and researchers. In this work, we employ the common independent competing risks framework, which presumes that the latent failure times corresponding to the two competing causes are mutually independent. Although this assumption greatly simplifies the formulation of the likelihood function and streamlines parameter estimation, it is a rather strong condition that may not reflect real-world scenarios. Future research could address this limitation by incorporating dependence structures through copula-based models. Copulas offer a flexible way to model dependence between risks while maintaining the clarity of the individual marginal distributions. Another future research avenue could investigate extending the model to handle more than two competing risks, especially in settings where sufficient labeled data and advanced computational tools are available. While such generalizations would broaden the model's applicability, they will also require careful attention to the increased complexity and challenges related to the parameters' identifiability.

Author contributions

Refah Alotaibi: Conceptualization, methodology, investigation, funding acquisition, writing original draft; Mazen Nassar: Conceptualization, methodology, investigation, writing review and editing; Ahmed Elshahhat: Software, Data curation, writing original draft. All authors read and approved the final manuscript.

Use of Generative-AI tools declaration

The authors declare that they have not used Artificial Intelligence (AI) tools in the creation of this article.

Funding

This research was funded by Princess Nourah bint Abdulrahman University Researchers Supporting Project number (PNURSP2025R50), Princess Nourah bint Abdulrahman University, Riyadh, Saudi Arabia.

Acknowledgement

The authors would like to express thank to the Editor-in-Chief and anonymous referees for their constructive comments and suggestions. This research was funded by Princess Nourah bint Abdulrahman University Researchers Supporting Project number (PNURSP2025R50), Princess Nourah bint Abdulrahman University, Riyadh, Saudi Arabia.

Data Availability

The authors confirm that the data supporting the findings of this study are available within the article.

Conflicts of interest

The authors declare no conflict of interest.

References

1. D. G. Hoel, A representation of mortality data by competing risks, *Biometrics*, **28** (1972), 475–488. https://doi.org/10.2307/2556161
2. M. J. Crowder, *Classical competing risks*, New York: Chapman and Hall/CRC, 2001. https://doi.org/10.1201/9781420035902
3. J. R. King, *Probability charts for decision making*, Industrial Press, 1971.
4. D. Kundu, N. Kannan, N. Balakrishnan, Analysis of progressively censored competing risks data, *Handbook of statistics*, **23** (2004), 331–348. https://doi.org/10.1016/S0169-7161(03)23018-2
5. M. Pintilie, Analysing and interpreting competing risk data, *Stat. Med.*, **26** (2007), 1360–1367. https://doi.org/10.1002/sim.2655
6. Z. Zhang, Survival analysis in the presence of competing risks, *Ann. Transl. Med.*, **5** (2017), 47. https://doi.org/10.21037/atm.2016.08.62
7. S. O. A. El-Azeem, M. H. Abu-Moussa, M. M. M. El-Din, L. S. Diab, On step-stress partially accelerated life testing with competing risks under progressive type-II censoring, *Ann. Data Sci.*, **11** (2024), 909–930. https://doi.org/10.1007/s40745-022-00454-0
8. Y. Tian, Y. Liang, W. Gui, Inference and optimal censoring scheme for a competing-risks model with type-II progressive censoring, *Math. Popul. Stud.*, **31** (2024), 1–39. https://doi.org/10.1080/08898480.2023.2225349
9. N. Balakrishnan, R. A. Sandhu, A simple simulational algorithm for generating progressive Type-II censored samples, *Am. Stat.*, **49** (1995), 229–230. https://doi.org/10.1080/00031305.1995.10476150
10. N. Balakrishnan, E. Cramer, U. Kamps, N. Schenk, Progressive type II censored order statistics from exponential distributions, *Statistics*, **35** (2001), 537–556. https://doi.org/10.1080/02331880108802753
11. M. K. Rastogi, Y. M. Tripathi, Estimating the parameters of a Burr distribution under progressive type II censoring, *Stat. Methodol.*, **9** (2012), 381–391. https://doi.org/10.1016/j.stamet.2011.10.002
12. S. Dey, L. Wang, M. Nassar, Inference on Nadarajah-Haghighi distribution with constant stress partially accelerated life tests under progressive type-II censoring, *J. Appl. Stat.*, **49** (2022), 2891–2912. https://doi.org/10.1080/02664763.2021.1928014
13. H. Krishna, R. Goel, Inferences for two Lindley populations based on joint progressive type-II censored data, *Commun. Stat. Simul. C.*, **51** (2022), 4919–4936. https://doi.org/10.1080/03610918.2020.1751851
14. Y. E. Jeon, S. B. Kang, J. I. Seo, Novel estimation based on a minimum distance under the progressive Type-II censoring scheme, *Commun. Stat. Appl. Met.*, **30** (2023), 411–421. https://doi.org/10.29220/CSAM.2023.30.4.411

15. R. Kumari, Y. M.Tripathi, L. Wang, R. K. Sinha, Reliability estimation for Kumaraswamy distribution under block progressive type-II censoring, *Statistics*, **58** (2024), 142–175. https://doi.org/10.1080/02331888.2024.2301736

16. H. K. T. Ng, D. Kundu, P. S. Chan, Type-II progress Statistical analysis of exponential lifetimes under an adaptive censoring scheme, *Nav. Res. Log.*, **56** (2009), 687–698. https://doi.org/10.1002/nav.20371

17. H. Panahi, S. Asadi, On adaptive progressive hybrid censored Burr type III distribution: Application to the nano droplet dispersion data, *Qual. Technol. Quant. M.*, **18** (2021), 179–201. https://doi.org/10.1080/16843703.2020.1806431

18. H. Haj Ahmad, M. M.Salah, M. S.Eliwa, Z. Ali Alhussain, E. M. Almetwally, E. A. Ahmed, Bayesian and non-Bayesian inference under adaptive type-II progressive censored sample with exponentiated power Lindley distribution, *J. Appl. Stat.*, **49** (2022), 2981–3001. https://doi.org/10.1080/02664763.2021.1931819

19. A. Elshahhat, M. Nassar, Analysis of adaptive Type-II progressively hybrid censoring with binomial removals, *J. Stat. Comput. Sim.*, **93** (2023), 1077–1103. https://doi.org/10.1080/00949655.2022.2127149

20. W. Yan, P. Li, Y. Yu, Statistical inference for the reliability of Burr-XII distribution under improved adaptive Type-II progressive censoring, *Appl. Math. Model.*, **95** (2021), 38–52. https://doi.org/10.1016/j.apm.2021.01.050

21. I. Elbatal, M. Nassar, A. Ben Ghorbal, L. S. G. Diab, A. Elshahhat, Reliability analysis and its applications for a newly improved type-II adaptive progressive alpha power exponential censored sample, *Symmetry*, **15** (2023), 2137. https://doi.org/10.3390/sym15122137

22. S. Dutta, S. Kayal, Inference of a competing risks model with partially observed failure causes under improved adaptive type-II progressive censoring, *P. I. Mech. Eng. O-J. Ris.*, **237** (2023), 765–780. https://doi.org/10.1177/1748006X221104555

23. M. Irfan, S. Dutta, A. K. Sharma, Statistical inference and optimal plans for improved adaptive type-II progressive censored data following Kumaraswamy-G family of distributions, *Phys. Scr.*, **100** (2025), 025213. https://doi.org/10.1088/1402-4896/ada216

24. A. Elshahhat, M. Nassar, Inference of improved adaptive progressively censored competing risks data for Weibull lifetime models, *Stat. Papers*, **65** (2024), 1163–1196. https://doi.org/10.1007/s00362-023-01417-0

25. W. I. Burr, Cumulative frequency distribution, *Ann. Math. Statist.*, **13** (1942), 215–232. https://doi.org/10.1214/aoms/1177731607

26. B. Tarvirdizade, H. K. G. H. K. Gharehchobogh, Inference on $Pr(X > Y)$ based on record values from the Burr type X distribution, *Hacet. J. Math. Stat.*, **45** (2016), 267–278.

27. A. Rabie, J. Li, E-Bayesian estimation for Burr-X distribution based on generalized type-I hybrid censoring scheme, *Am. J. Math. Manag. Sci.*, **39** (2020), 41–55. https://doi.org/10.1080/01966324.2019.1579123

28. M. Kayid, V. B. Nagarjuna, M. Elgarhy, Statistical inference for heavy-tailed Burr X distribution with applications, *J. Math.*, **2024** (2024), 9552629. https://doi.org/10.1155/2024/9552629

29. Y. Lio, D. G. Chen, T. R. Tsai, L. Wang, The reliability inference for multicomponent stress–strength model under the Burr X distribution, *AppliedMath*, **4** (2024), 394–426. https://doi.org/10.3390/appliedmath4010021

30. S. Dutta, S. Kayal, Analysis of the improved adaptive type-II progressive censoring based on competing risk data, 2021.

31. L. Wang, H. Li, Inference for exponential competing risks data under generalized progressive hybrid censoring, *Commun. Stat. Simul. C.*, **51** (2022), 1255–1271. https://doi.org/10.1080/03610918.2019.1667388

32. Y. Du, W. Gui, Statistical inference of Burr-XII distribution under adaptive type ii progressive censored schemes with competing risks, *Results Math.*, **77** (2022), 81. https://doi.org/10.1007/s00025-022-01617-4

33. A. S. Hassan, R. M. Mousa, M. H. Abu-Moussa, Bayesian analysis of generalized inverted exponential distribution based on generalized progressive hybrid censoring competing risks data, *Ann. Data Sci.*, **11** (2024), 1225–1264. https://doi.org/10.1007/s40745-023-00488-y

34. M. Plummer, N. Best, K. Cowles, K. Vines, CODA: convergence diagnosis and output analysis for MCMC, *R News*, **6** (2006), 7–11.

35. D. Kundu, N. Kannan, N. Balakrishnan, Analysis of progressively censored competing risks data, *Handbook of statistics*, **23** (2003), 331–348. https://doi.org/10.1016/S0169-7161(03)23018-2

36. R. Alotaibi, M. Nassar, Z. A. Khan, W. A. Alajlan, A. Elshahhat, Analysis and data modelling of electrical appliances and radiation dose from an adaptive progressive censored XGamma competing risk model, *J. Radiat. Res. Appl. Sci.*, **18** (2025), 101188. https://doi.org/10.1016/j.jrras.2024.101188

37. O. A. Alqasem, M. Nassar, M. E. Abd Elwahab, A. Elshahhat, Analyzing Burr-X competing risk model using adaptive progressive Type-II censored binomial removal data with application to electrodes and electronics, *J. Radiat. Res. Appl. Sci.*, **17** (2024), 101107. https://doi.org/10.1016/j.jrras.2024.101107

AIMS Press